AD-A100 620 DAVID W TAYLOR NAVAL SHIP RESEARCH AND DEVELOPMENT CE--ETC F/G 20/4
AN INTEGRAL PREDICTION METHOD FOR THREE-DIMENSIONAL TURBULENT B--ETC(U)
JUN 81 N C GROVES

UNCLASSIFIED DTNSRDC-81/050 NL

1 of 1
AD A100620

END
DATE FILMED
7 81
DTIC

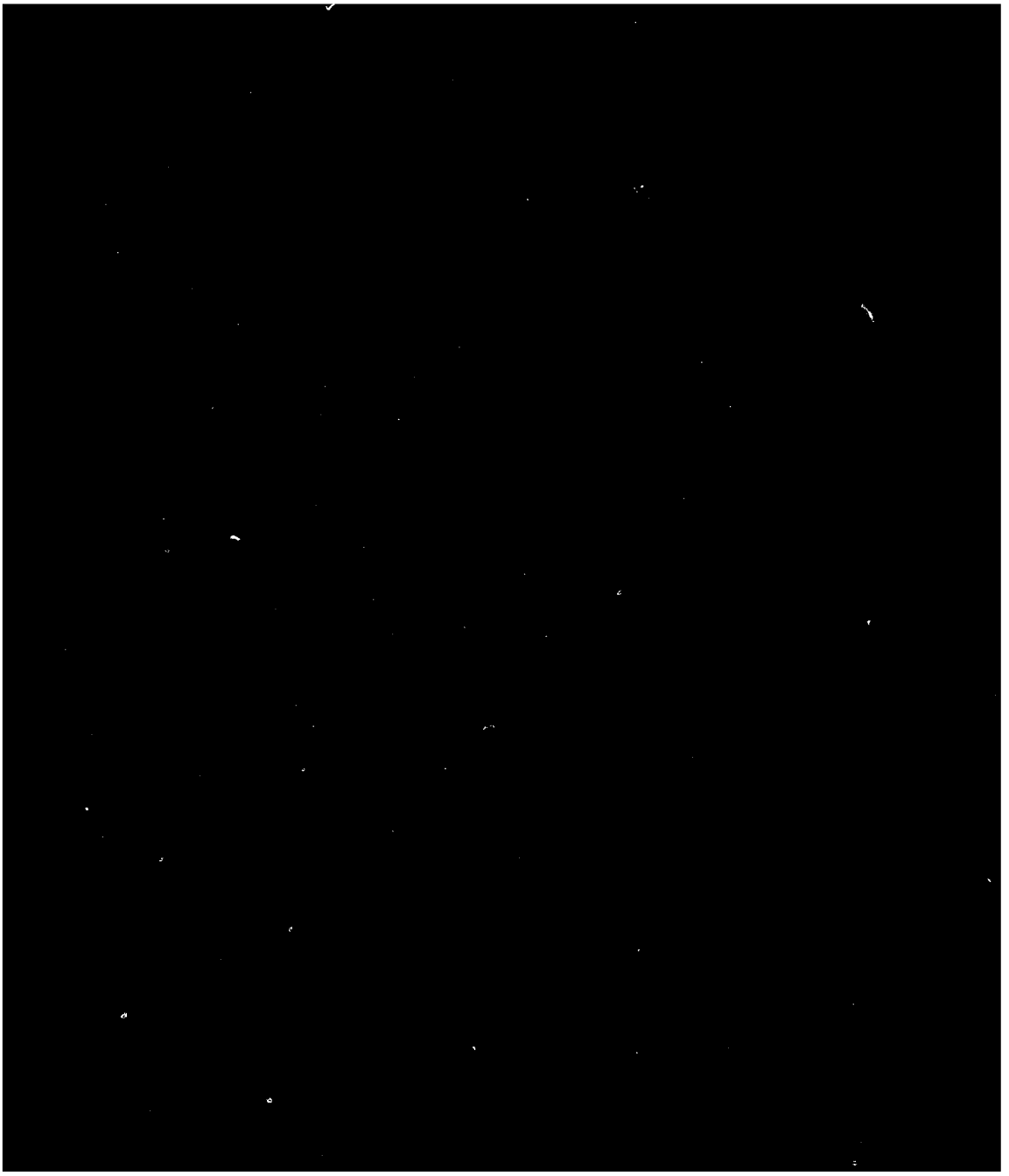

UNCLASSIFIED

SECURITY CLASSIFICATION OF THIS PAGE (When Data Entered)

REPORT DOCUMENTATION PAGE

READ INSTRUCTIONS BEFORE COMPLETING FORM

1. REPORT NUMBER: DTNSRDC-81/050	2. GOVT ACCESSION NO.: AD-A100620
3. RECIPIENT'S CATALOG NUMBER	
4. TITLE (and Subtitle): AN INTEGRAL PREDICTION METHOD FOR THREE-DIMENSIONAL TURBULENT BOUNDARY LAYERS ON ROTATING BLADES.	5. TYPE OF REPORT & PERIOD COVERED: Formal
	6. PERFORMING ORG. REPORT NUMBER
7. AUTHOR(s): Nancy C. Groves	8. CONTRACT OR GRANT NUMBER(s)
9. PERFORMING ORGANIZATION NAME AND ADDRESS: David W. Taylor Naval Ship Research and Development Center, Bethesda, Maryland 20084	10. PROGRAM ELEMENT, PROJECT, TASK AREA & WORK UNIT NUMBERS: Program Element 62543N; Task Area SF43421001; Work Unit 1500-104
11. CONTROLLING OFFICE NAME AND ADDRESS	12. REPORT DATE: Jun[redacted]81
	13. NUMBER OF PAGES
14. MONITORING AGENCY NAME & ADDRESS (if different from Controlling Office)	15. SECURITY CLASS. (of this report): UNCLASSIFIED
	15a. DECLASSIFICATION/DOWNGRADING SCHEDULE

16. DISTRIBUTION STATEMENT (of this Report)

APPROVED FOR PUBLIC RELEASE: DISTRIBUTION UNLIMITED

17. DISTRIBUTION STATEMENT (of the abstract entered in Block 20, if different from Report)

18. SUPPLEMENTARY NOTES

Paper presented at Propellers '81
Virginia Beach, Virginia
26-27 May 1981

19. KEY WORDS (Continue on reverse side if necessary and identify by block number)

Three-Dimensional
Turbulent Boundary Layers
Rotating Blades
Momentum Integral Equation
Entrainment Equation

20. ABSTRACT (Continue on reverse side if necessary and identify by block number)

A general formulation of the boundary-layer computation scheme on the surface of a rotating blade is presented. Momentum-integral methods, together with the three-dimensional entrainment equation for a rotating disk, are used to calculate the three-dimensional turbulent boundary layer in an orthogonal streamline coordinate system. First-order finite-difference methods are used to solve the resulting boundary-layer equations. The

(Continued on reverse side)

DD FORM 1 JAN 73 1473 EDITION OF 1 NOV 65 IS OBSOLETE
S/N 0102-LF-014-6601

UNCLASSIFIED
SECURITY CLASSIFICATION OF THIS PAGE (When Data Entered)

(Block 20 continued)

unknown variables are the streamwise momentum thickness, the shape parameter, and the streamline slope at the surface. The boundary-layer calculation method is combined with existing geometrical and inviscid potential-flow computer codes for rotating blades to form an efficient turbulent boundary-layer computer code. For a given potential-flow solution, a typical boundary-layer computation requires less than 10 seconds computer time on the Burroughs 7700 high-speed computer. Boundary-layer predictions are presented for several rotating blades. Computed results are shown to be in agreement with experimental data for a simple rotating body. For the examples considered, displacement of the mid-chord point of a blade from a straight radial line is predicted to reduce the computed values of local skin friction coefficient, with an estimated increase in overall efficiency of about one percentage point.

TABLE OF CONTENTS

	Page
LIST OF FIGURES	iv
TABLE	iv
NOTATION	v
ABSTRACT	1
INTRODUCTION	2
COORDINATE REFERENCE FRAMES	5
BASIC EQUATIONS	6
MOMENTUM EQUATIONS	6
ENTRAINMENT EQUATION	9
ADDITIONAL RELATIONSHIPS	9
SKIN FRICTION	10
VELOCITY PROFILES	11
CROSSWISE THICKNESSES	11
ENTRAINMENT FUNCTION	12
NUMERICAL ANALYSIS	13
COMPUTATIONAL RESULTS AND DISCUSSION	17
BLADE 1	18
BLADES 2	21
CONCLUDING REMARKS	32
ACKNOWLEDGMENTS	34
REFERENCES	34
APPENDIX - COMPUTATIONAL RESULTS FOR BLADES 2 AT A FULL-SCALE REYNOLDS NUMBER	37

LIST OF FIGURES

Page

1 - Blade Surface Geometry. 5

2 - Streamline Grid on a Typical Rotating Sector. 16

3 - Points at Which Calculations Performed. 17

4 - Geometry and Coordinates of Rotating Helical Sector 19

5 - Variation of Momentum Thickness θ_{11} on Rotating Helical Blade 22

6 - Variation of Limiting Streamline Angle β on Rotating Helical Blade. . . . 23

7 - Variation of Skin Friction Coefficient C_f on Rotating Helical Blade . . . 24

8 - Computed Streamline Grid for Blades 2A, 2B, and 2C. 26

9 - Computed Distribution of Momentum Thickness θ_{11} Along Streamline 14 of Warped and Unwarped Blades 28

10 - Computed Distribution of Tangent of Limiting Streamline Angle β Along Streamline 14 of Warped and Unwarped Blades 29

11 - Computed Distribution of Shape Parameter H Along Streamline 14 of Warped and Unwarped Blades 30

12 - Computed Distribution of Local Skin Friction Coefficient C_f Along Streamline 14 of Warped and Unwarped Blades 31

13 - Effect of Warp and Skew on Predicted Values of Local Skin Friction Coefficient C_f 40

Table 1 - Geometry of Rotating Blade 2B. 25

NOTATION

A	Known coefficient matrix for streamwise partial derivatives in the numerical solution procedure
B	Known coefficient matrix for crosswise partial derivatives in the numerical solution procedure
C	Known right-hand side matrix in the numerical solution procedure
C_{f_1}	Wall skin friction coefficient in the streamwise ξ-direction, $$C_{f_1} = \left(\mu\frac{\partial u}{\partial \zeta} - \varrho\overline{u'w'}\right) \Big/ \left(\frac{1}{2}\varrho U^2\right)$$
C_{f_2}	Wall skin friction coefficient in the crosswise η-direction, $$C_{f_2} = \left(\mu\frac{\partial v}{\partial \zeta} - \varrho\overline{v'w'}\right) \Big/ \left(\frac{1}{2}\varrho U^2\right)$$
D	Rotor diameter
ds	Element of length in orthogonal streamline coordinates, $$ds^2 = h_1^2 d\xi^2 + h_2^2 d\eta^2 + h_3^2 d\zeta^2$$
F	Dimensionless entrainment function, $$F = 0.025\left(\frac{G}{G-2} - 1\right)$$
G	Function of the shape parameter H, $$G = 2H/(H - 1)$$

H	Streamwise shape parameter, $H = \delta_1/\theta_{11}$
h_1	Metric coefficient for the ξ-coordinate
h_2	Metric coefficient for the η-coordinate
h_3	Metric coefficient for the ζ-coordinate (taken to be unity)
i	Superscript which references the crosswise (η) direction in the numerical solution procedure
J_v	Advance coefficient, $J_v = V/(nD)$
j	Superscript which references the streamwise (ξ) direction in the numerical solution procedure
K_1	Geodesic curvature of lines of constant ξ, $$K_1 = \frac{1}{h_1 h_2}\frac{\partial h_1}{\partial \eta}$$
K_2	Geodesic curvature of lines of constant η, $$K_2 = \frac{1}{h_1 h_2}\frac{\partial h_2}{\partial \xi}$$
n	Rotational speed
R	Rotor tip radius
R_n	Reynolds number based on 0.7-radius, $$R_n = (\text{Chord})_{0.7}\, V\sqrt{1+\left(\frac{0.7\pi}{J_v}\right)^2}\Big/\nu$$
R_x	Local Reynolds number, $R_x = Ux/\nu$
$R_{\theta_{11}}$	Reynolds number based on the streamwise momentum thickness, $$R_{\theta_{11}} = U\theta_{11}/\nu$$
r	Variable in the radial direction
U	Speed along the streamline at the outer edge of the boundary layer
u	Time-mean velocity component in the ξ-direction

$\overline{u'w'}, \overline{v'w'}$	Time-averaged products of the turbulent fluctuating velocity components in the ξ and η-directions, respectively (i.e., components of the Reynolds stresses)
V	Reference speed
v	Time-mean velocity component in the η-direction
W	Unknown vector in the numerical solution procedure
w	Time-mean velocity component in the ζ-direction
x_c	Fraction of chord, measured from leading edge
x_R	Nondimensional radius, fraction of tip radius
z	Variation in the axial direction
β	Angle between the direction of the wall friction vector and the inviscid streamline
δ	Boundary-layer thickness
δ_1	Streamwise displacement thickness, $\delta_1 = \int_0^\delta (1 - \frac{u}{U}) d\zeta$
δ_2	Crosswise displacement thickness, $\delta_2 = -\int_0^\delta \frac{v}{U} d\zeta$
ζ	Distance along the surface normal
η	Independent variable along surface and normal to the streamlines
θ	Independent cylindrical coordinate (see Figure 1)
θ_{11}	Streamwise momentum thickness, $\theta_{11} = \int_0^\delta (1 - \frac{u}{U}) \frac{u}{U} d\zeta$

θ_{12} Crosswise momentum thickness,

$$\theta_{12} = \int_o^\delta \left(1 - \frac{u}{U}\right) \frac{v}{U} \, d\zeta$$

θ_{21} Crosswise momentum thickness,

$$\theta_{21} = -\int_o^\delta \frac{uv}{U^2} \, d\zeta = \delta_2 + \theta_{12}$$

θ_{22} Crosswise momentum thickness,

$$\theta_{22} = -\int_o^\delta \frac{v^2}{U^2} \, d\zeta$$

μ Fluid viscosity

ν Kinematic viscosity of fluid, $\nu = \mu/\varrho$

ξ Independent variable along streamlines

ϱ Fluid density

ω Rotational speed, $\omega = 2\pi n$

ω_3 Angular velocity component in the ζ-direction

ABSTRACT

A general formulation of the boundary-layer computation scheme on the surface of a rotating blade is presented. Momentum-integral methods, together with the three-dimensional entrainment equation for a rotating disk, are used to calculate the three-dimensional turbulent boundary layer in an orthogonal streamline coordinate system. First-order finite-difference methods are used to solve the resulting boundary-layer equations. The unknown variables are the streamwise momentum thickness, the shape parameter, and the streamline slope at the surface. The boundary-layer calculation method is combined with existing geometrical and inviscid potential-flow computer codes for rotating blades to form an efficient turbulent boundary-layer computer code. For a given potential-flow solution, a typical boundary-layer computation requires less than 10 seconds computer time on the Burroughs 7700 high-speed computer. Boundary-layer predictions are presented for several rotating blades. Computed results are shown to be in agreement with experimental data for a simple rotating body. For the examples considered, displacement of the mid-chord point of a blade from a straight radial line is predicted to reduce the computed values of local skin friction coefficient, with an estimated increase in overall efficiency of about one percentage point.

INTRODUCTION

Turbulent boundary layers occur in practice on the rotating blades of compressors, turbines, helicopters, or propulsors. Centrifugal and Coriolis forces are additional terms that arise in the governing equations due to the blade rotation relative to the description of non-rotating systems. These forces, along with the pressure and viscous forces, result in a complex three-dimensional flow configuration.

Several previous studies have been made of turbulent boundary layers on rotating bodies. One of the earliest studies was by von Kármán[1] in 1946 on axisymmetric bodies. Banks and Gadd[2], in 1962, investigated *both laminar and turbulent* boundary layers on rotating blades. A review of much of the recent work is given by Meyne[3] (1972).

In 1969, Cham and Head[4] presented experimental and theoretical turbulent boundary-layer results on a rotating disk. *In following years, they extended* their theory to include the flows over a rotating circular cylinder in an axial stream[5] and a rotating axisymmetric body[6]. All three of Cham and Head's investigations used the momentum integral[7] with entrainment[8] method of solution. The assumed *entrainment function and the* exact form of the momentum integral equations varied with the differing geometries. Good agreement was found between theoretical predictions and experimental results for Cham and Head's investigations.

Lakshminarayana, et al.[9] presented *results of an investigation* of the turbulent boundary layer on a rotating helical blade in 1972. Again, the solution was based on the momentum integral method. The governing equations were simplified by the assumptions of zero pressure

gradient and the use of the orthogonal streamline coordinate system. Overall, their theoretical predictions were in acceptable agreement with their experimental results: measured values of the streamwise momentum thickness were no more than 20 percent less than predictions at midradius and values of the limiting streamline were in ± 2 degrees agreement with predictions.

Also in 1972, Meyne[3] presented theoretical and experimental results for boundary-layer flow on rotating wedged-shaped surfaces. Meyne sought a generalized similarity solution (reducing the equations to an ordinary differential equation in the normal direction) and considered both laminar and turbulent flow. Detailed results are shown for the predicted boundary-layer parameters for laminar flow. However, his equations for the turbulent flow case were identical to those of Banks and Gadd[2] and thus no new information was obtained.

The present work extends that of the previous investigators by providing for theoretical computations of the turbulent boundary layer that develops about more complex geometries. In particular, the current method was designed to compute the turbulent boundary layer on the surfaces of rotating blades with thickness and loading in an axial stream operating at 0.7-radius Reynolds numbers greater than about 4×10^6 for which fully turbulent flow is expected. Although not considered explicitly, the present calculation method could be modified slightly to perform the laminar calculation as well.

The three-dimensional turbulent boundary layer in streamline coordinates (ξ, η, ζ) is governed by three equations. These are the ξ *and* η *momentum integral equations* and the continuity equation. These equations are the same as those given by Smith[10] and by Cumpsty and Head[11] with one additional term (to account for the rotation) in both of the momentum integral equations. In the integral method, the equations of motion are integrated across the boundary layer, producing first-order partial differential equations. Empirical information is incorporated in the equations to account for Reynolds stresses. In the numerical method, direct use is made of the streamwise momentum thickness θ_{11} and the shape parameter H, the two parameters which most readily characterize the behavior of turbulent boundary layers[12]. The

use of streamline coordinates simplifies both the boundary conditions and the governing equations but requires the definition of a new coordinate system based on the flow field and blade geometry.

Several assumptions, which are discussed in a later section of this paper, are made concerning the behavior of the flow. These assumptions reduce the number of unknown quantities in the three governing equations to three variables. These are the streamwise momentum thickness θ_{11}, the shape parameter H, and the tangent of β, the angle between the direction of the wall friction vector (or wall streamline) and the inviscid streamline.

When computing the turbulent boundary layer on a rotating blade with thickness and lift, a potential-flow computer code[13] developed at DTNSRDC by Brockett is used. This code computes the potential flow velocities, slopes of the streamlines and crosswise-normal lines, metric coefficients, and the angular velocity component normal to the surface. All values are given in non-dimensional coordinates (x_c, x_R) where x_c is the chord fraction, measured from the leading edge and x_R is the fraction of radius, measured from the axis of rotation.

Streamlines and crosswise-normal lines are determined from the given slopes using an Euler-predictor/trapezoidal-corrector method[14]. Potential-flow velocities, metric coefficients, etc. are interpolated in the streamline coordinate system using a spline-under-tension method[15]. A first-order finite-difference approximation[16] is used to solve the system for the three basic unknown quantities.

No interaction with the hub is considered in the present analysis and the nature of the flow near the tip is assumed to be adequately predicted by the potential-flow model.

Results of the turbulent boundary-layer calculation are presented for several rotating geometries. The first body studied is the rotating, weakly helical, segment investigated experimentally and analytically by Lakshminarayana, et al.[9]. Computed results are in agreement with the experimental data. The remaining geometries are described analytically with no previous experimental or analytical boundary-layer data available. The effect of blade warp and skew on

the predicted values of the local skin-friction coefficient is investigated qualitatively using these surfaces. Blade warp is defined as the angular displacement of the midchord point from the reference line in the plane of rotation and blade skew is defined as the displacement of the mid-chord point along the pitch helix at constant radius.

COORDINATE REFERENCE FRAMES

The geometry and boundary-layer characteristics of rotating blades are described by two coordinate systems fixed in the rotating surface. Brockett[13] gives the geometry and potential flow characteristics in terms of the non-dimensional coordinates x_c and x_R, see Figure 1. These are non-orthogonal, helical coordinates where x_c is the fraction of chord as measured from the leading edge and x_R is the fraction of radius as measured from the axis of rotation.

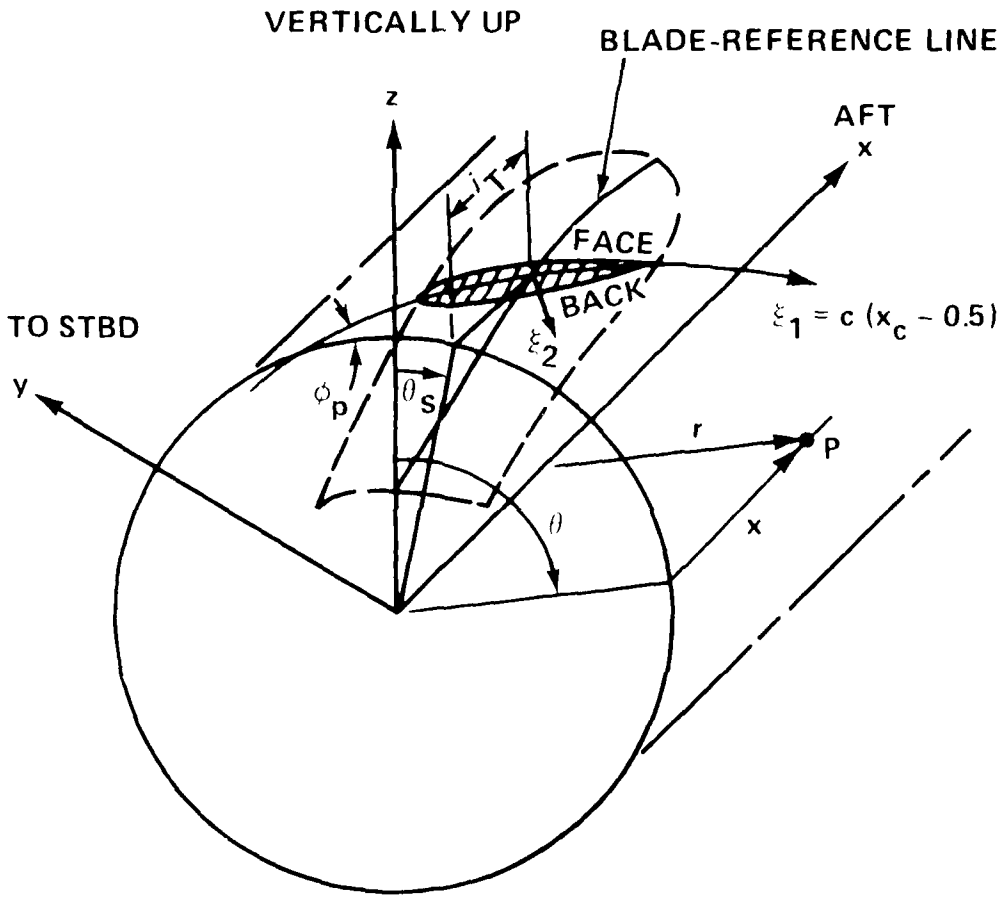

Figure 1. Blade Surface Geometry

The turbulent boundary-layer scheme uses an orthogonal, curvilinear coordinate system based on the potential-flow streamlines, but with explicit dependence on the x_c and x_R coordinates. The use of the orthogonal coordinates simplifies the boundary conditions and, hence, the boundary-layer equations governing the turbulent flow. The orthogonal streamline coordinates on the surface are ξ, which varies along streamlines, and η, which is normal to the streamline. The ζ coordinate measures distance along the surface normal.

In the orthogonal, curvilinear coordinates, the distance between lines of constant ξ or η varies from point to point on the surface. Metric coefficients, denoted by h_1, h_2, and h_3 for the ξ, η, and ζ coordinates, respectively, are required to correlate surface distances to increments of the streamline coordinates. Since the boundary-layer thickness is assumed to be small and the ζ coordinate is assumed to measure distance along the surface normal, the metric h_3 can be set equal to unity with no loss of generality. A general element of length ds in streamline coordinates is then given by

$$ds^2 = h_1{}^2 d\xi^2 + h_2{}^2 d\eta^2 + d\zeta^2 \tag{1}$$

where h_1 and h_2 are functions of ξ and η only.

BASIC EQUATIONS

Momentum Equations

The continuity and momentum equations for laminar flow in a rotating system are readily available in the literature, e.g., Moore[17]. The turbulent boundary-layer equations are the laminar equations plus additional terms due to the Reynolds stresses. In streamline coordinates, the equations for turbulent flow are

Continuity:
$$\frac{\partial(h_2 u)}{\partial \xi} + \frac{\partial(h_1 v)}{\partial \eta} + \frac{\partial(h_1 h_2 w)}{\partial \zeta} = 0 \tag{2a}$$

ξ-Momentum:
$$\frac{u}{h_1}\frac{\partial u}{\partial \xi} + \frac{v}{h_2}\frac{\partial u}{\partial \eta} + w\frac{\partial u}{\partial \zeta} + uvK_1 - v^2K_2 \quad 2\omega_3 v \tag{2b}$$
$$= -\frac{U}{h_1}\frac{\partial U}{\partial \xi} + \frac{1}{\rho}\frac{\partial}{\partial \zeta}\left(\mu\frac{\partial u}{\partial \zeta} - \rho\,\overline{u'w'}\right)$$

η-Momentum:
$$\frac{u}{h_1}\frac{\partial v}{\partial \xi} + \frac{v}{h_2}\frac{\partial v}{\partial \eta} + w\frac{\partial v}{\partial \zeta} + uvK_2 - (u^2 - U^2)K_1 + 2\omega_3(u - U) = \frac{1}{\varrho}\frac{\partial}{\partial \zeta}\left(\mu\frac{\partial v}{\partial \zeta} - \varrho\,\overline{v'w'}\right) \tag{2c}$$

where u, v, and w are the time-mean velocity components in the ξ, η and ζ directions, respectively,

K_1 is the geodesic curvature of lines of constant ξ,

$$K_1 = \frac{1}{h_1 h_2}\frac{\partial h_1}{\partial \eta}$$

K_2 is the geodesic curvature of lines of constant η,

$$K_2 = \frac{1}{h_1 h_2}\frac{\partial h_2}{\partial \xi}$$

U is the speed along the streamline at the outer edge of the boundary layer,

μ is the viscosity of the fluid,

ϱ is the density of the fluid,

ω_3 is the angular velocity component in the ζ-direction ($\underline{n}$-direction)

$$\omega_3 = \underline{\omega} \cdot \underline{n} = -\omega(\underline{i} \cdot \underline{n})$$

$\overline{u'w'}$ and $\overline{v'w'}$ are the time averaged products of the turbulent fluctuating velocity components (i.e., components of the Reynolds stresses).

The integral boundary-layer equations are obtained by integrating the momentum equations with respect to ζ from the surface of the blade ($\zeta = 0$) to the edge of the boundary-layer ($\zeta = \delta$). The continuity equation is used to eliminate all terms involving the velocity component w, normal to the blade surface. The resulting equations[10] are:

ξ-momentum integral:
$$\frac{1}{h_1}\frac{\partial \theta_{11}}{\partial \xi} + \frac{1}{h_2}\frac{\partial \theta_{12}}{\partial \eta} + K_2(\theta_{11} - \theta_{22}) + K_1(2\theta_{21} - \delta_2) + \frac{2\theta_{21} - \delta_2}{Uh_2}\frac{\partial U}{\partial \eta} + \frac{2\theta_{11} + \delta_1}{Uh_1}\frac{\partial U}{\partial \xi} - \frac{2\omega_3}{U}\delta_2 = \frac{1}{2}C_{f_1} \tag{3a}$$

η-momentum integral: $$\frac{1}{h_1}\frac{\partial \theta_{21}}{\partial \xi} + \frac{1}{h_2}\frac{\partial \theta_{22}}{\partial \eta} + 2\theta_{21}\left(\frac{1}{Uh_1}\frac{\partial U}{\partial \xi} + K_2\right) + \frac{2\omega_3}{U}\delta_1 + \frac{2\theta_{22}}{Uh_2}\frac{\partial U}{\partial \eta} - K_1(\theta_{11} - \theta_{22} + \delta_1) = \frac{1}{2}C_{f_2} \tag{3b}$$

In equations 3a and 3b, θ_{11}, θ_{12}, θ_{21}, θ_{22}, δ_1, and δ_2 are the momentum and displacement thicknesses defined, respectively, by succeeding equations 5a through 5f and

$$C_{f_1} = \frac{\mu\frac{\partial u}{\partial \zeta} - \rho\overline{u'w'}}{\frac{1}{2}\rho U^2} \text{ and } C_{f_2} = \frac{\mu\frac{\partial v}{\partial \zeta} - \rho\overline{v'w'}}{\frac{1}{2}\rho U^2} \tag{4}$$

are the turbulent wall skin friction coefficient components in the ξ and η directions, respectively.

The momentum and displacement thicknesses are defined by:

$$\theta_{11} = \int_0^\delta \left(1 - \frac{u}{U}\right)\frac{u}{U}\,d\zeta \tag{5a}$$

$$\theta_{12} = \int_0^\delta \left(1 - \frac{u}{U}\right)\frac{v}{U}\,d\zeta \tag{5b}$$

$$\theta_{21} = -\int_0^\delta \frac{uv}{U^2}\,d\zeta \tag{5c}$$

$$\delta_2 = \theta_{12}$$

$$\theta_{22} = -\int_0^\delta \frac{v^2}{U^2}\,d\zeta \tag{5d}$$

$$\delta_1 = \int_0^\delta \left(1 - \frac{u}{U}\right)d\zeta \tag{5e}$$

$$\delta_2 = -\int_0^\delta \frac{v}{U}\,d\zeta \tag{5f}$$

The boundary conditions are $u = v = 0$ at $\zeta = 0$ and $u = U$, $v = 0$ at $\zeta = \delta$, the edge of the boundary-layer.

The two momentum integral equations are insufficient to define the boundary-layer development. An additional equation (the entrainment equation) will be introduced in the next section and several assumptions (for C_{f_1}, C_{f_2}, and mean velocity profile shapes) applied in order to reduce the number of unknown quantities to three. These three quantities are the streamwise momentum thickness, θ_{11}; the shape factor parameter, H; and the tangent of the angle between surface streamline and external streamline directions, $\tan\beta$.

Entrainment Equation

The three-dimensional entrainment equation of Myring[8], which has also been used by Cumptsy and Head[11] and von Kerczek and Langan[18], is the additional equation used here to describe the turbulent boundary-layer flow over the blade surface. This equation describes the growth of the boundary layer with time as the turbulent mixing process spreads the general motion of turbulent flow[19]. The continuity equation is integrated with respect to ζ through the boundary layer to obtain (in streamline coordinates) the entrainment equation:

$$\frac{1}{h_1}\frac{\partial(\delta-\delta_1)}{\partial\xi} - \frac{1}{h_2}\frac{\partial\delta_2}{\partial\eta} + \left(\frac{1}{Uh_1}\frac{\partial U}{\partial\xi} + K_2\right)(\delta-\delta_1) - \delta_2\left(\frac{1}{h_2U}\frac{\partial U}{\partial\eta} + K_1\right) = \frac{1}{h_1}\frac{\partial\delta}{\partial\xi} - \frac{w(\delta)}{U} \tag{6a}$$

The right-hand side of equation (6a) is a measure of the rate at which fluid enters the boundary layer. Denoting this quantity by F, where F is a dimensionless entrainment function, the entrainment equation becomes:

$$\frac{1}{h_1}\frac{\partial(\delta-\delta_1)}{\partial\xi} - \frac{1}{h_2}\frac{\partial\delta_2}{\partial\eta} + \left(\frac{1}{Uh_1}\frac{\partial U}{\partial\xi} + K_2\right)(\delta-\delta_1) - \delta_2\left(\frac{1}{h_2U}\frac{\partial U}{\partial\eta} + K_1\right) = F \tag{6b}$$

Details of the entrainment function are given in a later section of this paper.

ADDITIONAL RELATIONSHIPS

Further assumptions are needed in order to solve the two momentum integral equations (3a and 3b) and the entrainment equation (6a).

Skin Friction

The turbulent skin friction terms C_{f_1} and C_{f_2} on the right-hand side of the ξ and η momentum integral equations, respectively, are obtained from empirical data for the skin friction coefficient C_f in the local inviscid streamline direction[18] by

$$C_{f_1} = C_f \tag{7a}$$

and

$$C_{f_2} = C_f \tan\beta \tag{7b}$$

where

$$\tan\beta = \lim_{\zeta \to o} \frac{v}{u} = \lim_{\zeta \to o} \frac{\frac{\partial v}{\partial \zeta}}{\frac{\partial u}{\partial \zeta}} \tag{7c}$$

By assuming that the component of boundary-layer flow in the inviscid streamline direction is approximately two-dimensional, the skin friction coefficient C_f can be specified using a two-dimensional skin friction formula. The skin friction relationship given by Thompson[20] and approximated by Head and Patel[21] is used in the present calculation method. The skin friction coefficient is approximated by the analytic relation

$$C_f = \exp(aH + b) \tag{8a}$$

where

$$a = 0.019521 - 0.386768c + 0.028345c^2 - 0.000701c^3 \tag{8b}$$

$$b = 0.191511 - 0.834891c + 0.062588c^2 - 0.001953c^3 \tag{8c}$$

$$c = \ln R_{\theta_{11}} \tag{8d}$$

$$H = \frac{\delta_1}{\theta_{11}} \tag{8e}$$

$$R_{\theta_{11}} = \frac{U\theta_{11}}{\nu} \tag{8f}$$

U = speed at the edge of boundary layer (8g)

ν = kinematic viscosity of water (8h)

θ_{11} = the dimensional streamline component of the momentum thickness. (8i)

Both coefficients a and b decrease as θ_{11} increases. Thus, for decreases or "small" increases in the shape factor H, the skin friction coefficient C_f decreases as θ_{11} increases.

Velocity Profiles

Assumptions involving the formulation of the streamwise and crosswise velocity profiles are made in order to relate the crosswise momentum and displacement thicknesses θ_{12}, θ_{21}, θ_{22}, and δ_2 to the streamwise momentum and displacement thicknesses θ_{11} and δ_1. Extreme accuracy is not necessary in the representation of these velocity profiles since they are used only to relate integrated values of the crosswise and streamwise momentum and displacement thicknesses.

The approximation for the streamwise velocity profile is given by Cooke[22] and by Patel[23]. This formulation, which approximates the experimental swept-wing boundary-layer data of Wallace[24], is

$$\frac{u}{U} = \left(\frac{\zeta}{\delta}\right)^{\frac{H-1}{2}} \tag{9a}$$

The crosswise velocity profiles are assumed to be related to the streamwise velocity profiles by empirical formulation due to Mager[25]. This approximation, also assumed by Cooke[22], Cham and Head[4], and von Kerczek and Langan[18], is given by the relation

$$\frac{v}{U} = \frac{u}{U}\left(1 - \frac{\zeta}{\delta}\right)^2 \tan\beta \tag{9b}$$

This approximation is assumed to be adequate as long as it is not applied to crossflow reversal.

An approximation for the boundary-layer thickness δ is found by substituting the assumed form of the streamwise velocity profile, equation (9a), into the definition of the streamwise momentum thickness θ_{11}, equation (5a). Integration and simplification give the approximation

$$\delta = \theta_{11}\left(\frac{2H}{H-1} + H\right) \tag{9c}$$

Crosswise Thicknesses

The expressions for streamwise velocity profile, equation (9a), and the crosswise velocity profile, equation (9b) are substituted into the definitions of the streamwise displacement thickness and the crosswise momentum and displacement thicknesses, equations (5b) through

(5f), and integrated across the boundary layer. After considerable manipulations, the following expressions result:

$$\theta_{12} = \theta_{11} M_{12} \tag{10a}$$

$$\theta_{21} = \theta_{11} M_{21} \tag{10b}$$

$$\theta_{22} = \theta_{11} M_{22} \tag{10c}$$

$$\delta_1 = \theta_{11} D_1 \tag{10d}$$

$$\delta_2 = \theta_{11} D_2 \tag{10e}$$

where $$M_{12} = -(G+H)\tan\beta \left(\frac{1}{H} - \frac{4}{H+1} + \frac{1}{H+2} + \frac{4}{H+3} - \frac{2}{H+5} \right) \tag{11a}$$

$$M_{21} = -(G+H)\tan\beta \left(\frac{1}{H} - \frac{2}{H+1} + \frac{1}{H+2} \right) \tag{11b}$$

$$M_{22} = -(G+H)\tan^2\beta \left(\frac{1}{H} - \frac{4}{H+1} + \frac{6}{H+2} - \frac{4}{H+3} + \frac{1}{H+4} \right) \tag{11c}$$

$$D_1 = H \tag{11d}$$

$$D_2 = -(G+H)\tan\beta \left(\frac{2}{H+1} - \frac{4}{H+3} + \frac{2}{H+5} \right) \tag{11e}$$

Entrainment Function

The entrainment function F is assumed to be determined uniquely by the circumferential velocity profile in the same way as proposed by Head[19] for a two-dimensional boundary layer. However, Cham and Head[4] found that if the entrainment function is reduced to approximately two-thirds of the flat plate value, then agreement between calculated turbulent boundary-layer development on a rotating disk and experiments was excellent. Incorporating the results of Cham and Head into the entrainment function presented by Green, et al.[26] gives the following universal expression for the function F:

$$F = 0.025 \left(\frac{G}{G-2} - 1 \right) \tag{12a}$$

$$G = \frac{2H}{H-1} \tag{12b}$$

$$H = \text{the shape factor parameter, } H \equiv \frac{\delta_1}{\theta_{11}} \tag{12c}$$

The relationship between the boundary-layer thickness δ and the streamwise momentum thickness θ_{11} given in equation (9c) can be rewritten using the definition of G as

$$\delta = \theta_{11}\,(G + H) \tag{12d}$$

The three basic equations which characterize the turbulent flow over the surface of the rotating segment (the momentum integral equations (3a) and (3b) and the entrainment equation (6b)) are now expressed in terms of the three basic unknown quantities: the streamwise momentum thickness θ_{11}, the shape factor parameter H, and the tangent of the angle between surface streamline and external streamline directions, $t = \tan\beta$.

NUMERICAL ANALYSIS

In order to obtain a more compact form of the three basic equations, (3a), (3b), and (6b), the expressions for the crosswise momentum and displacement thicknesses and the streamwise displacement thickness, equations (10a) through (10e), are substituted into each of these equations. After some manipulation, the single hyperbolic equation in vector form becomes

$$A(W(\xi,\eta))\,\frac{\partial W}{\partial \xi} + B(W(\xi,\eta))\,\frac{\partial W}{\partial \eta} = C(W) \tag{13}$$

The unknown vector W is given by

$$W = \begin{pmatrix} W_1 \\ W_2 \\ W_3 \end{pmatrix} = \begin{pmatrix} \theta_{11} \\ t \\ H \end{pmatrix} \tag{14a}$$

and the known coefficient matrices are

$$A(W) = \begin{pmatrix} \frac{1}{h_1} & 0 & 0 \\ \frac{M_{21}}{h_1} & \frac{\theta_{11}}{h_1}\frac{\partial M_{21}}{\partial t} & \frac{\theta_{11}}{h_1}\frac{\partial M_{21}}{\partial H} \\ \frac{G+H-D_1}{h_1} & \frac{\theta_{11}}{h_1}\frac{\partial (G+H-D_1)}{\partial t} & \frac{\theta_{11}}{h_1}\frac{\partial (G+H-D_1)}{\partial H} \end{pmatrix} \tag{14b}$$

$$B(W) \begin{pmatrix} \frac{M_{12}}{h_2} & \frac{\theta_{11}}{h_2}\frac{\partial M_{12}}{\partial t} & \frac{\theta_{11}}{h_2}\frac{\partial M_{12}}{\partial H} \\ \frac{M_{22}}{h_2} & \frac{\theta_{11}}{h_2}\frac{\partial M_{22}}{\partial t} & \frac{\theta_{11}}{h_2}\frac{\partial M_{22}}{\partial H} \\ -\frac{D_2}{h_2} & -\frac{\theta_{11}}{h_2}\frac{\partial D_2}{\partial t} & -\frac{\theta_{11}}{h_2}\frac{\partial D_2}{\partial H} \end{pmatrix} \tag{14c}$$

$$C(W) = \begin{pmatrix} C_1 \\ C_2 \\ C_3 \end{pmatrix} \tag{14d}$$

$$C_1 = \frac{1}{2} C_{f_1} - K_2\theta_{11}(1-M_{22}) - K_1\theta_{11}(2M_{21}-D_2) - \frac{\theta_{11}(2M_{21}-D_2)}{U h_2}\frac{\partial U}{\partial \eta} - \frac{\theta_{11}(2+D_1)}{U h_1}\frac{\partial U}{\partial \xi} + \frac{2\omega_3}{U}\theta_{11}D_2 \tag{14e}$$

$$C_2 = \frac{1}{2} C_{f_2} - 2\theta_{11}M_{21}\left(\frac{1}{h_1 U}\frac{\partial U}{\partial \xi} + K_2\right) - \frac{2\omega_3}{U}\theta_{11}D_1 - \frac{2\theta_{11}M_{22}}{h_2 U}\frac{\partial U}{\partial \eta} + K_1\theta_{11}(1-M_{22}+D_1) \tag{14f}$$

$$C_3 = F - \theta_{11}(G+H-D_1)\left(\frac{1}{U h_1}\frac{\partial U}{\partial \xi} + K_2\right) + \theta_{11}D_2\left(\frac{1}{h_2 U}\frac{\partial U}{\partial \eta} + K_1\right) \tag{14g}$$

Since equation (13) is hyperbolic, the entire solution between asymptotes could be determined once initial conditions were specified along these limiting lines. Initial conditions, however, are not readily available for the geometries of interest. Therefore, a solution procedure is adopted which yields results only along one side of the bisector of the asymptotes and requires initial conditions along only one asymptote.

A first-order finite difference approximation is used to solve equation (13) in the streamline coordinates (ξ, η). The grid spacing is given by $\Delta\xi$ in the streamwise direction and $\Delta\eta$ in the crosswise direction. Arclengths are approximated by the chordlength; hence, reasonably small increments are required. Superscript i refers to the crosswise (η) direction and superscript j refers to the streamwise (ξ) direction. Forward differencing in ξ yields

$$\left(\frac{\partial W}{\partial \xi}\right)^{j} = \frac{W^{j+1} - W^{j}}{\Delta\xi} \tag{15a}$$

and backward differencing in η yields

$$\left(\frac{\partial W}{\partial \eta}\right)^{i} = \frac{W^{i} - W^{i-1}}{\Delta\eta} \tag{15b}$$

If the values of θ_{11}, H, and $\tan\beta$ are known at the grid node (i,j), the values of these three variables can be found at the node (i,j + 1) by the first order finite difference approximation

$$A^{i,j}\left(\frac{W^{i,j+1} - W^{i,j}}{\Delta\xi}\right) + B^{i,j}\left(\frac{W^{i,j} - W^{i-1,j}}{\Delta\eta}\right) \quad C^{i,j} \tag{16}$$

If the $A^{i,j}$ matrix is nonsingular, equation (16) can be solved for $W^{i,j+1}$:

$$W^{i,j+1} = \Delta\xi(A^{i,j})^{-1}C^{i,j} - \frac{\Delta\xi}{\Delta\eta}\left[(A^{i,j})^{-1}B^{i,j}(W^{i,j} - W^{i-1,j})\right] + W^{i,j} \tag{17}$$

where $\Delta\xi = \xi^{j+1} - \xi^{j}$ (18a)

and $\Delta\eta = \eta^{i} - \eta^{i-1}$ (18b)

The streamline grid is shown on a typical sector rotating at a constant angular speed ω in Figure 2. As experiments indicate[3], streamlines (lines along which ξ varies) are shown to approximate constant radius lines and the crossflow lines (lines along which η varies) are shown to approximate radial lines. Streamlines are indicated by the variable j and crossflow lines by the variable i. The arclengths $\Delta\xi$ and $\Delta\eta$ are shown to vary from point to point on the sector surface. Grid nodes, which are defined as intersections of streamlines and crossflow lines, are labeled i,j for i = 1 to N, j = 1 to M where N = number of streamlines and M = number of crossflow lines.

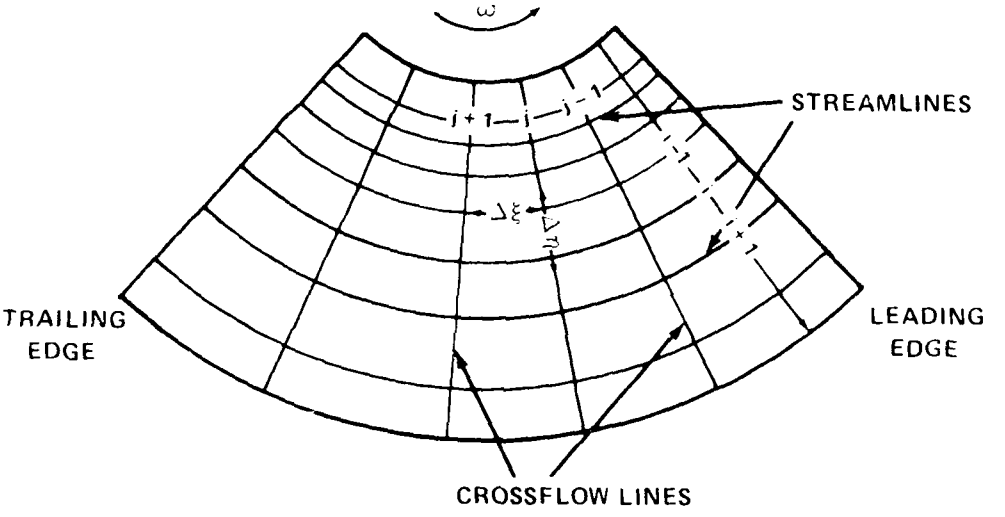

Figure 2. Streamline Grid on a Typical Rotating Sector

Figure 3 shows the calculation sequence for the turbulent boundary layer on a typical sector. For convenience, the grid nodes used in the calculation procedure are numbered sequentially from the number 1. It is assumed that starting values of θ_{11}, H, and $t = \tan\beta$ are given along a crossflow line, points numbered 1-7. Turbulent boundary-layer characteristics are solved along successive crossflow lines as indicated by the increasing numbers in Figure 3. For example, data at points 1 and 2 are used to obtain predictions at point 8, data at points 2 and 3 are used for predictions at point 9, etc. As can be seen from this simplified example of the calculation procedure, a fine grid is necessary near the hub of the blade in order to obtain results near the trailing edge.

A blade is typically defined by a grid containing about 250 nodes. Experience to date indicates that grid nodes should be distributed on the blade with a greater concentration near the inner radii and leading edge; and arclengths $\Delta\xi$ and $\Delta\eta$ should increase uniformly in the directions of the trailing edge and tip of the blade. Using the Burroughs 7700 high-speed computer, the boundary-layer computation for this grid requires less than 10 seconds computer time at a cost of less than one dollar.

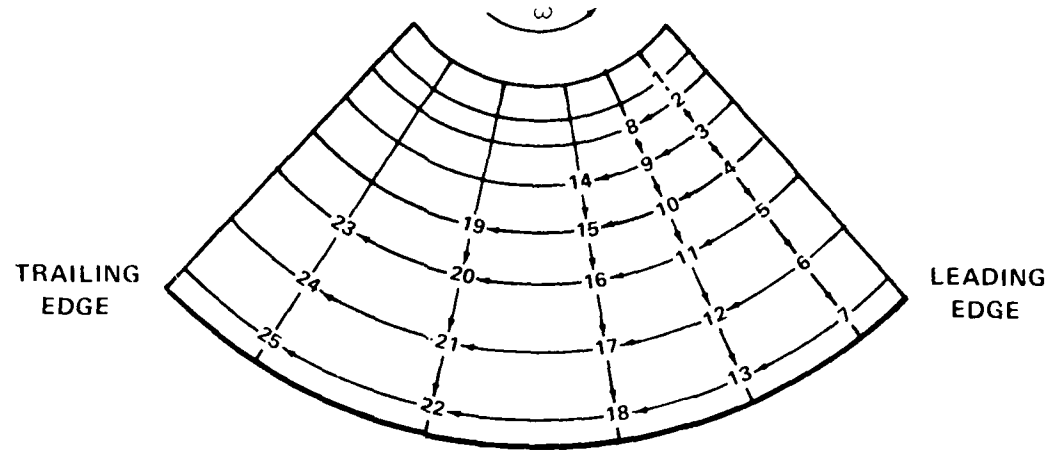

Figure 3. Points at Which Calculations Performed

COMPUTATIONAL RESULTS AND DISCUSSION

The computer code for calculating the three-dimensional turbulent boundary layer has been evaluated using several geometries for which analytical and experimental data are available. Among these are a flat plate, a two-dimensional foil, a rotating disk, and a rotating helical blade. Excellent agreement with test data was found in each case. The turbulent boundary layer was computed for the rotating helical blade assuming both zero and nonzero crossflow. As was anticipated, results of these two computations showed agreement within 15 percent. Results are presented for only the more complex of these geometries, the rotating helical blade with nonzero crossflow. The turbulent boundary-layer development over the surface of Blade 1, a sector of 300 degrees included angle, was investigated experimentally and analytically by

Lakshminarayana, et al.[9]. The small pitch of the sector was not included in their analysis, nor is it included in the present investigation.

The effect of blade warp and skew is investigated using three blades: an unskewed Blade 2A, a 72 degree warped Blade 2B and a 72 degree skewed Blade 2C. Blades 2 are analytically-defined lifting surfaces for which no previous experimental or analytical turbulent boundary-layer data exist. Details of the geometry and potential flow calculations are given in Reference 13. Initial conditions for this geometry are assumed to be flat plate and rotating disk values for turbulent flow. The computed local skin friction coefficients are compared for these blades. At present, only the skin friction coefficients are computed. In the future, it is anticipated that the force and moment values will also be computed, allowing a calculation of the effect of viscous drag on overall performance.

Blade 1

The turbulent boundary-layer characteristics were investigated initially on a single non-lifting rotating helical sector of 92.6 cm (36.6 in.) diameter with a 300 degree included angle, hence of a large chord length. Both experimental and analytical data are available from Lakshminarayana, et al.[9] for comparison.

The pitch of the helical surface studied by Lakshminarayana, et al.[9] was 25.4 cm (10 inches), for a pitch-diameter ratio of 0.273. Thus, the geometry can be approximated by a flat circular disk with a leading and trailing edge 300 degrees apart. The blade was mounted on a 22.86 cm (0.75 ft) radius hub and the maximum radius of the blade was 46.48 cm (1.525 ft). The blade was enclosed in a housing wall with a 0.20 cm (0.08 in.) clearance between the blade tip and the wall. The free-stream onset flow was zero and the rotational speed of the blade, denoted ω, remained constant at 47 rad/s (450 rev/min). The geometry of the sector is shown in Figure 4.

The theoretical analysis of Lakshminarayana, et al.[9] is based on a rotating system described with cylindrical coordinates (r, θ, z) where r varies in the radial direction, θ varies in the chordwise direction (i.e., circumferential direction) and z varies along the surface normal (axial direction). These coordinates are indicated in Figure 4 and are used when comparing the experimental data with the results of the present theory.

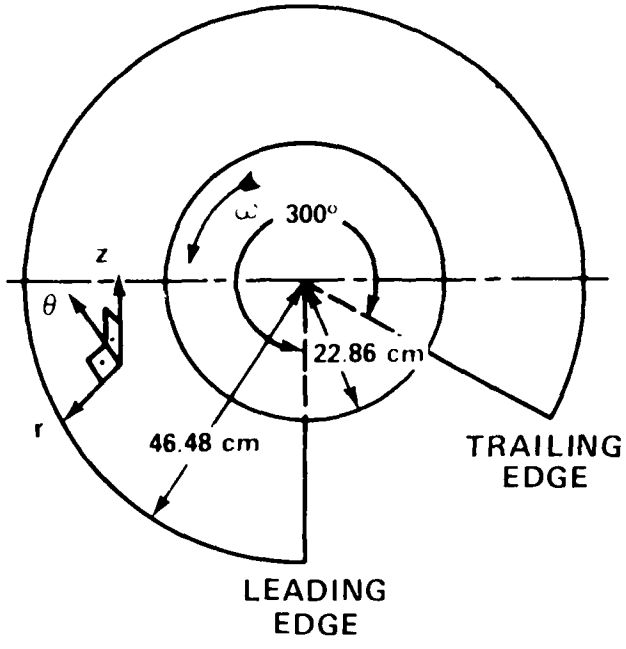

Figure 4. Geometry and Coordinates of Rotating Helical Sector

The potential-flow surface velocity for Blade 1 is simply ωr along the chordlines. The streamlines are lines of constant radius along which neither the potential flow velocity nor the metric coefficient $h_2 = R$ varies. The momentum integral and entrainment equations for this sector are thus simplified to:

ξ-momentum integral:

$$\frac{1}{h_1}\frac{\partial \theta_{11}}{\partial \xi} + \frac{1}{h_2}\frac{\partial \theta_{12}}{\partial \eta} + K_1(2\theta_{21} - \delta_2) + \frac{2\theta_{21} - \delta_2}{U h_2}\frac{\partial U}{\partial \eta} = \frac{2\omega_3}{U}\delta_2 \quad \frac{1}{2}C_{f1} \tag{19a}$$

η-momentum integral:

$$\frac{1}{h_1}\frac{\partial \theta_{21}}{\partial \xi} + \frac{1}{h_2}\frac{\partial \theta_{22}}{\partial \eta} + \frac{2\omega_3}{U}\delta_1 + \frac{2\theta_{22}}{U h_2}\frac{\partial U}{\partial \eta} \quad K_1(\theta_{11} \quad \theta_{22} + \delta_1) \quad \frac{1}{2}C_{f2} \tag{19b}$$

Entrainment:

$$\frac{1}{h_1}\frac{\partial(\delta \delta_1)}{\partial \xi} - \frac{1}{h_2}\frac{\partial \delta_2}{\partial \eta} - \left(\frac{1}{U h_2}\frac{\partial U}{\partial \eta} + K_1\right) \delta_2 \quad \text{I} \tag{19c}$$

The metric coefficients h_1 and h_2 are the chord length and maximum radius, respectively and ξ and η are the changes in the fraction of chord and fraction of radius, respectively. Substitution

of these values into equations (19a) and (19b) yields the momentum integral equations given by Lakshminarayana, et al.[9]. In their analytical study, only the streamwise momentum thickness θ_{11} and the limiting streamline angle β varied. A general form of the solution was assumed (θ_{11} was assumed to vary with radius and chord and tanβ was assumed to vary with θ_{11} only) and the governing momentum integral equations solved numerically using the fourth-order Runge-Kutta method. In reference (9), it was assumed that the streamwise velocity profile varies as the 1/7 power of (ζ/δ) and a simple friction formula was selected. The present method also uses the entrainment equation and a different solution method based on assumed entrainment and skin friction relationships and assumed velocity profiles. Thus, some differences occur in the predicted flow parameters.

Lakshminarayana, et al.[9] presented experimental and theoretical results at a rotational speed of 47 rad/s (450 rev/min). The kinematic viscosity ν equaled 1.486×10^{-5} m^2/s (160×10^{-6} ft^2/sec) which corresponded to air at 20°C (68°F). These conditions, for a Reynolds number based on tip radius and tip rotational speed of 7×10^5 (or a 0.7-radius Reynolds number of 2.5×10^6 (see next section for definitions)), are used in the evaluation of the present method.

In the numerical solution procedure, Lakshminarayana, et al.[9] performed calculations of the laminar boundary layer until the flat-plate critical Reynolds number, $R_x = \omega r^2\theta/\nu = 3 \times 10^5$, was reached. The values of the streamwise momentum thickness θ_{11} and limiting streamline angle β were then used as initial conditions for the turbulent calculations. Flow visualization experiments using a sublimation technique supported the use of the flat plate critical Reynolds number to determine the transition point.

With the present scheme, calculations began at the location $\theta = 0.733$ radians and $x_R/R = 0.492$, the grid node location closest to the experimentally-determined transition location. Initial conditions for the streamwise momentum thickness θ_{11} and the tangent of the limiting streamline β were obtained from the experimental data of Lakshminarayana, et al.[9], but no radial variations were considered. Initial values were taken to be $\theta_{11} = 0.24$ mm (0.0008 ft), tan$\beta = 0.2$, and $H = 1.5$ at each radial location along the chordwise position $\theta = 0.733$ radians.

Figures 5 through 7 present the results of the turbulent boundary-layer calculation over the surface of Blade 1. Both the experimental and analytical results of Lakshminarayana, et al.[9] and flat plate predictions (adjusted for the region of laminar flow prior to $\theta = 0.733$ radians) are indicated in the figures for comparison. The variation in the streamwise momentum thickness θ_{11} is given in Figures 5a through 5c at the radial locations $x_R = r/R = 0.72$, 0.82, 0.93, respectively. The momentum thickness is predicted to be less than the flat-plate value given by Prandlt's[27] approximation[1] ($\theta_{11} = 0.036 \times R_x^{-1/5}$, with $U = \omega r$ and $x = r\theta$), and less than the prediction of Lakshminarayana, et al.[9]. Use of the present theory gives satisfactory agreement with the experimental results.

The computed variation of the limiting streamline angle β is shown in Figure 6a for r/R = 0.74 and in Figure 6b for r/R = 0.965. The peak in the surface flow angle at the leading edge is the result of laminar flow. The present calculations start at $\theta = 0.733$ radians (42 degrees), the measured point of transition at r/R = 0.72. These figures show that the currently-applied analytical model predicts greater variations in the limiting streamline angle than observed for the measured data. The laminar sublayer is not included in the present calculations and may be important for this variable. Values near the tip may be influenced by the annular wall.

The distribution of the local skin friction coefficient for varying radial locations is given in Figure 7a at $\theta = 2.64$ radians and Figure 7b at $\theta = 4.76$ radians. Flat plate predictions were made using the Schoenherr[28] curve for local skin friction, $C_f = 0.310 \{\ln^2(2R_\theta) + 2\ln(2R_\theta)\}$. Figure 7 shows that the measured values of the local skin friction coefficient are larger than the flat plate predictions and smaller than the experimental predictions.

Blades 2

In this section, results are presented for the computed boundary-layer characteristics on three analytically-defined blades[13]: an unwarped propulsor, Blade 2A (similar to NSRDC Model 4381), a highly warped propulsor, Blade 2B (similar to NSRDC Model 4498), and a

[1] Prandlt's approximation was adjusted for the region of laminar flow by matching the values of laminar and turbulent momentum thickness θ_{11} at the location $\theta = 0.733$ radians.

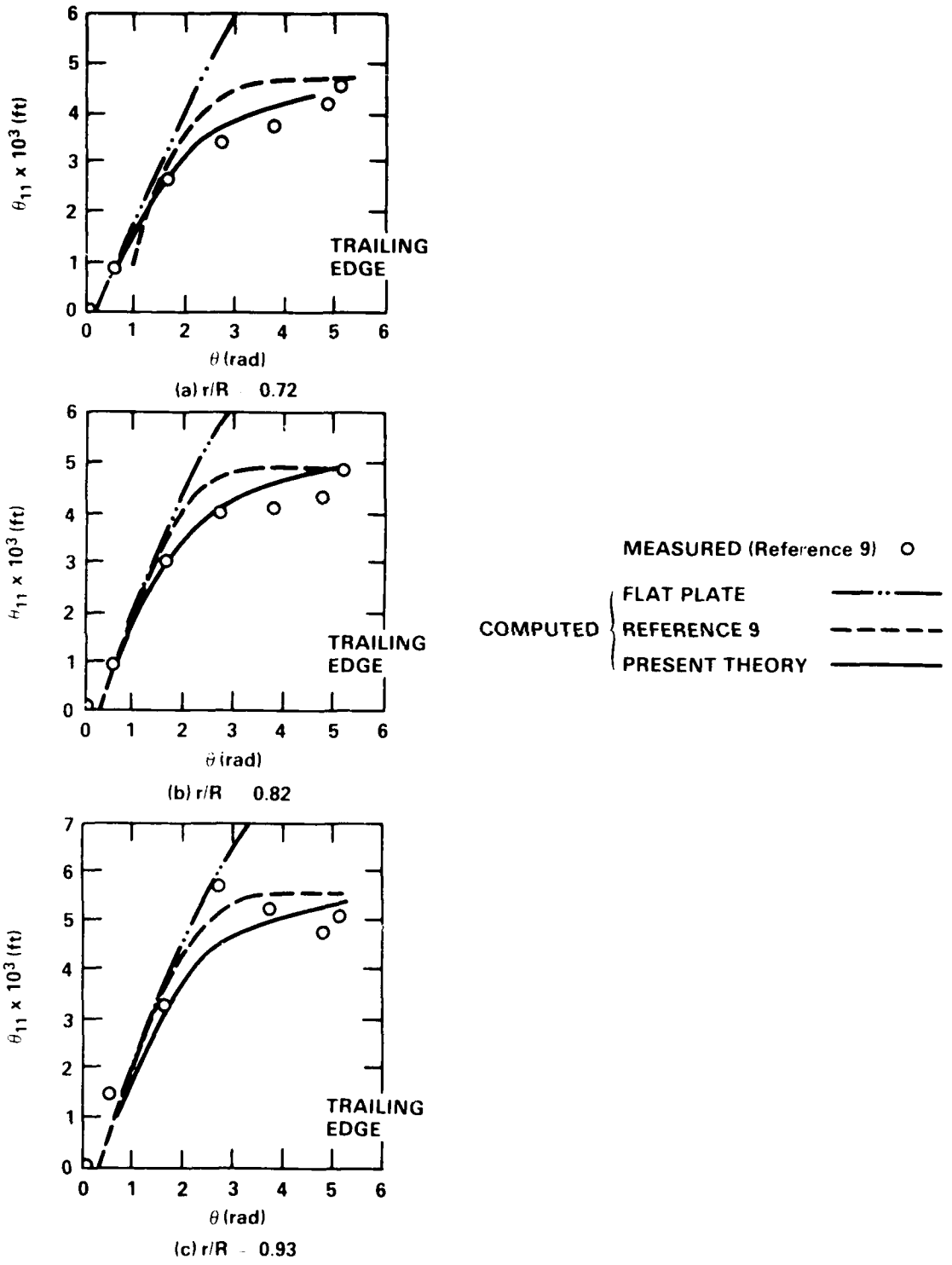

Figure 5. Variation of Momentum Thickness θ_{11} on Rotating Helical Blade.

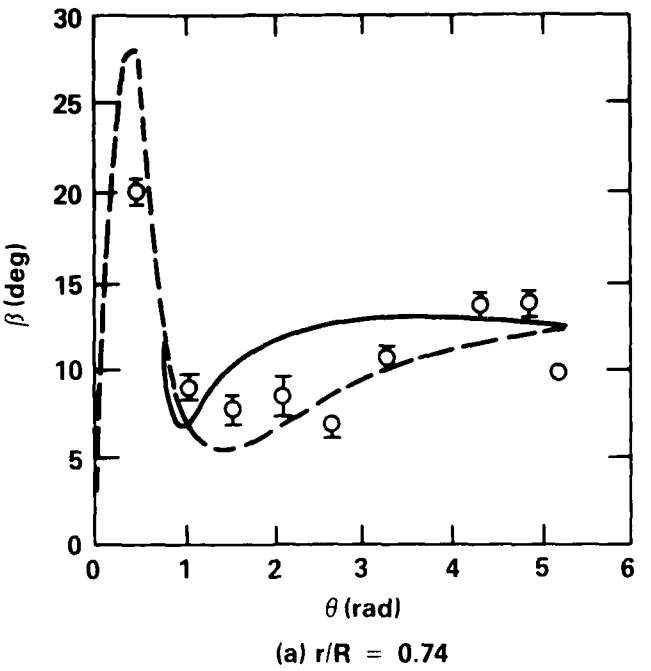

(a) r/R = 0.74

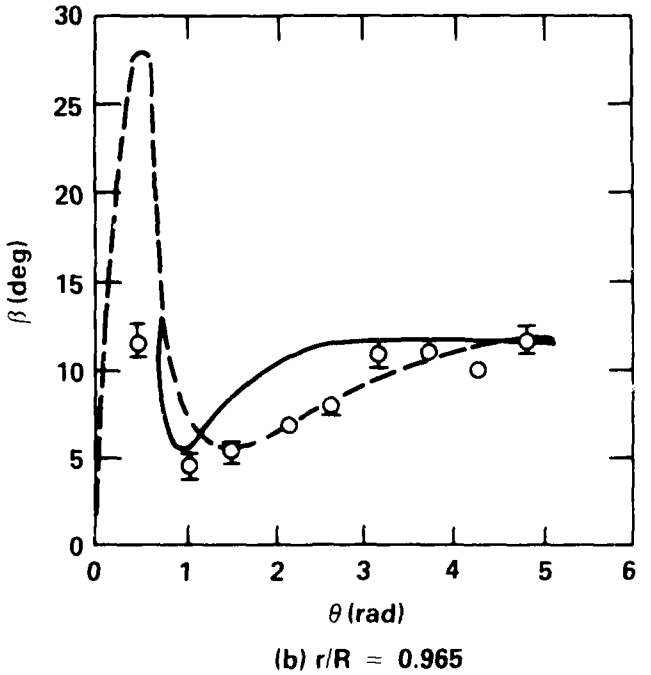

(b) r/R = 0.965

Figure 6. Variation of Limiting Streamline Angle β on Rotating Helical Blade

highly-skewed propulsor, Blade 2C (similar to NSRDC Model 4383). Of particular interest is the effect of warp on the values of the computed skin-friction coefficients.

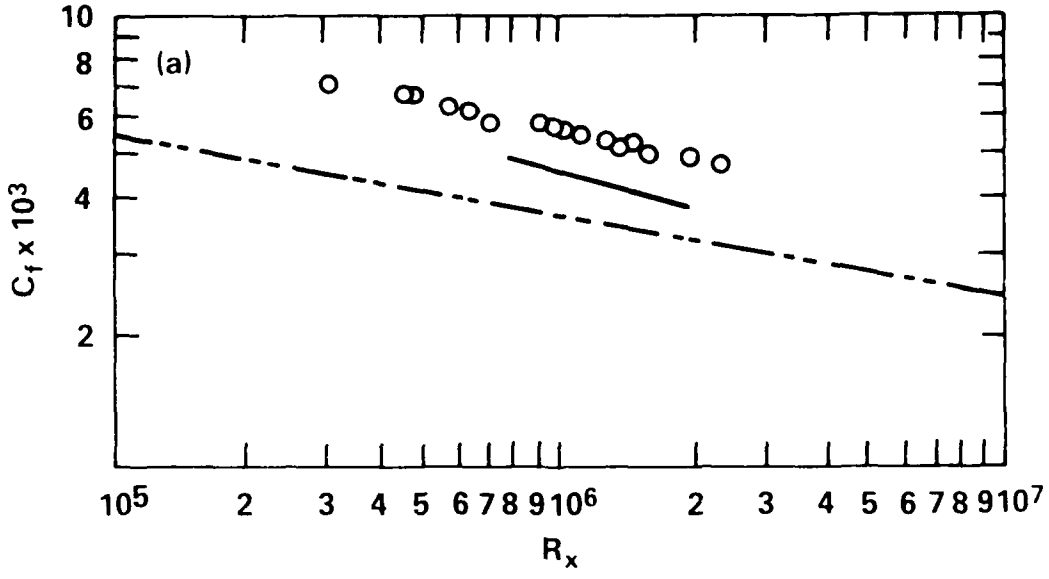

(a) θ = 2.64 RAD

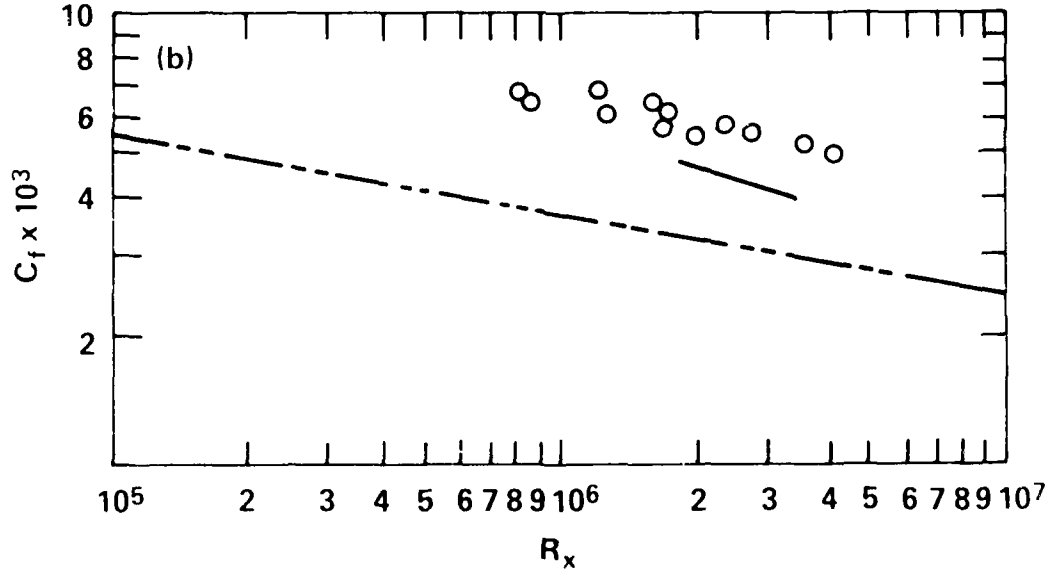

(b) θ = 4.76 RAD

MEASURED (Reference 9) ○

COMPUTED — SCHOENHERR FLAT PLATE ----

COMPUTED — PRESENT THEORY ——

Figure 7. Variation of Skin Friction Coefficient C_f on Rotating Helical Blade.

The geometry of the warped blade is given in Table 1. The geometry of the unwarped blade is identical with the exception that the skew angles are zero. The blades rotate about a cylindrical hub at a constant angular velocity ω in a constant axial onset stream of speed V.

TABLE 1 — GEOMETRY OF ROTATING BLADE 2B

Fraction of Radius	Chord / Diameter	Pitch / Diameter	Skew Angle (radians)	Thickness / Chord
0.20000	0.16500	1.49500	0.00000	0.24000
0.25000	0.19700	1.53500	0.07854	0.19800
0.30000	0.22900	1.54400	0.15708	0.15610
0.40000	0.27500	1.48700	0.31416	0.10680
0.50000	0.31200	1.38900	0.47124	0.07680
0.60000	0.33700	1.27700	0.62832	0.05650
0.70000	0.34700	1.15600	0.78540	0.04210
0.80000	0.33400	1.04200	0.94248	0.03140
0.90000	0.28000	0.93400	1.09956	0.02460
0.95000	0.24000	0.87700	1.17810	0.02330
1.00000	0.00000	0.81200	1.25664	0.02460

Fraction of Chord	Thickness Offset	Chordwise Loading	
0.000000	0.000000	0.000000	
0.007596	0.086824	0.912003	
0.030154	0.171010	0.992645	
0.066987	0.250000	1.040899	
0.116978	0.321394	1.074103	
0.178606	0.383022	1.097916	
0.250000	0.433013	1.114882	
0.328990	0.469846	1.126317	
0.413176	0.492404	1.132938	
0.500000	0.500000	1.135109	
0.586824	0.492202	1.135109	
0.671010	0.467219	1.135109	
0.750000	0.421900	1.103578	
0.821349	0.354824	0.949248	
0.883022	0.269637	0.712632	
0.933013	0.176665	0.450324	
0.969846	0.091629	0.216717	
0.992404	0.031655	0.056755	Number of Blades 5
1.000000	1.010000	0.000000	Design J_λ = 0.889

Unpublished experimental results at DTNSRDC on a similar geometry indicate that the flow over the blades will be fully turbulent at a 0.7-radius Reynolds number of 4×10^6. A 0.7-radius Reynolds number is defined as:

$$R_n = \frac{(c)_{0.7} V \sqrt{1 + \left(\frac{0.7\pi}{J_\lambda}\right)^2}}{\nu} \qquad (20)$$

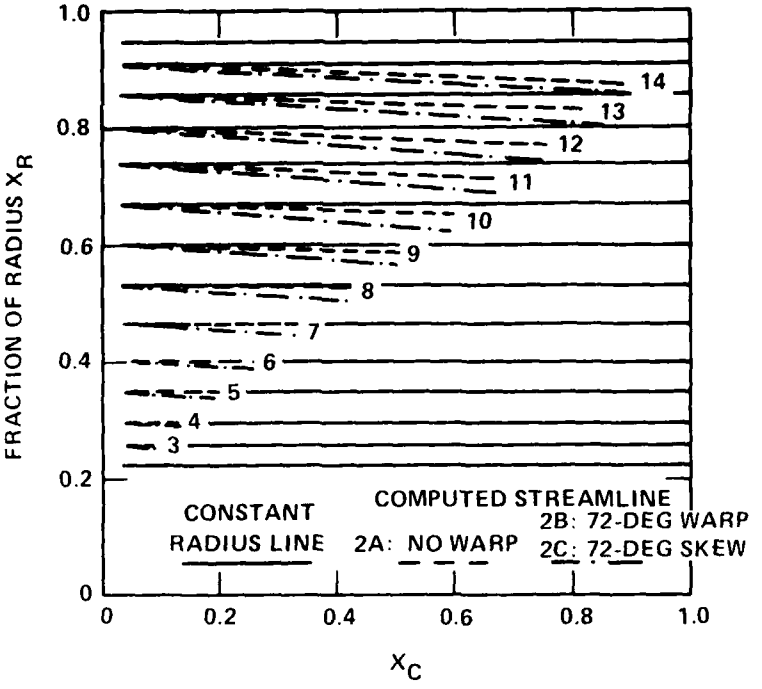

(a) SUCTION SURFACE

NOTE: STREAMLINES 13 AND 14 ARE SAME FOR SEGMENTS 2A, 2B, AND 2C

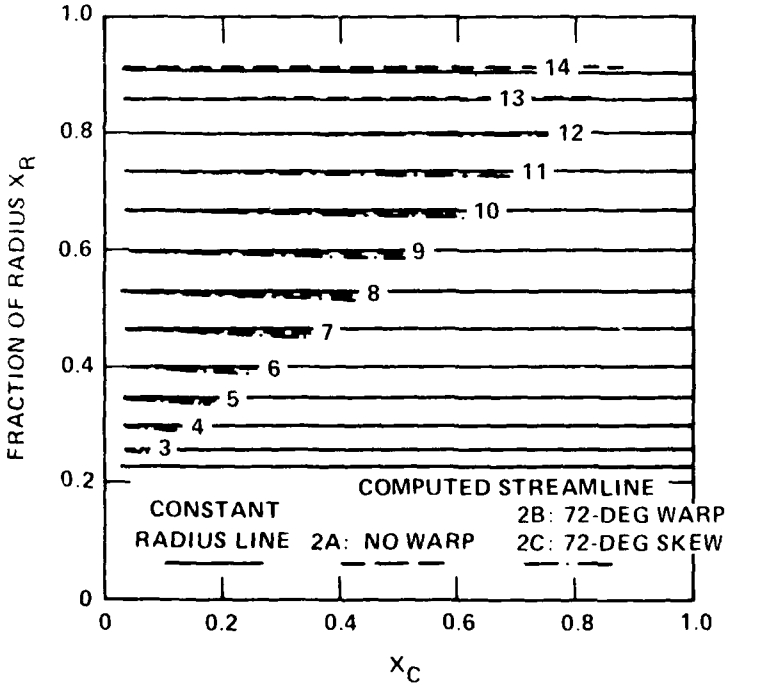

(b) PRESSURE SURFACE

Figure 8. Computed Streamline Grid for Blades 2A, 2B, and 2C.

where: $(c)_{0.7}$ = blade chord at 0.7 radius
V = onset speed
J_v = advance coefficient, $J_v = V/(nD)$
n = constant rotational speed, revolutions per unit time
D = rotor diameter
ν = kinematic viscosity

The assumed flow conditions for turbulent flow are $\nu = 1.191 \times 10^{-6} m^2/s$ (1.282×10^{-5} ft^2 sec), V = 16.9 m/s (55.3 ft/sec), and $\omega = 391.5$ rad/s.

No previous analytical or experimental boundary-layer results exist for these specific blades. Initial conditions are assumed to be determined by flat-plate values for turbulent flow[28,29,30], with[2] $\theta_{11} = \nu\ U\ 0.0142\ (R_X)^{6/7}$, $C_f = 0.310/[\ln^2(2R_\theta) + 2\ln(2R_\theta)]$, and $H = 1/[1-4.67(C_f)^{1/2}]$, and by the rotating disk limiting streamline angle β value[4], $\beta = +11$ degrees on the blade suction surface and $\beta = -11$ degrees on the blade pressure surface. Because of the uncertainty in these starting values, the computed results are of qualitative, but not necessarily quantitative, validity.

The computed potential-flow streamlines for the blades are shown in Figure 8. The streamlines for the warped Blade 2B and the skewed Blade 2C coincide and both are shown by the dashed line in Figure 8. Streamlines at increased radial values lie noticeably inboard of the constant radius lines on the suction surface. Except near the tip, the same trend is evident on the pressure surface. Streamlines 13 and 14 coincide on the pressure surface of the three blades.

The computed boundary-layer characteristics on the three blades show similar trends along each streamline. Therefore, the results will be presented only along one streamline, streamline 14. Figures 9 through 11 show the computed distributions of θ_{11}, $\tan\beta$, and H, respectively. Increased values of the streamwise momentum thickness θ_{11} and the shape parameter H are predicted for the warped and skewed blades relative to the unskewed blade.

Figure 12 shows the predicted distribution of the local skin friction coefficient C_f, as computed by empirical relationships given in Equations (8), for Blades 2A, 2B, and 2C. The significant result shown in this figure is that the local skin friction coefficient is predicted to be reduced on both the suction and pressure surfaces when the blade is highly warped or skewed. Reduc

[2] R_X (chord) (fraction of chord) U/ν

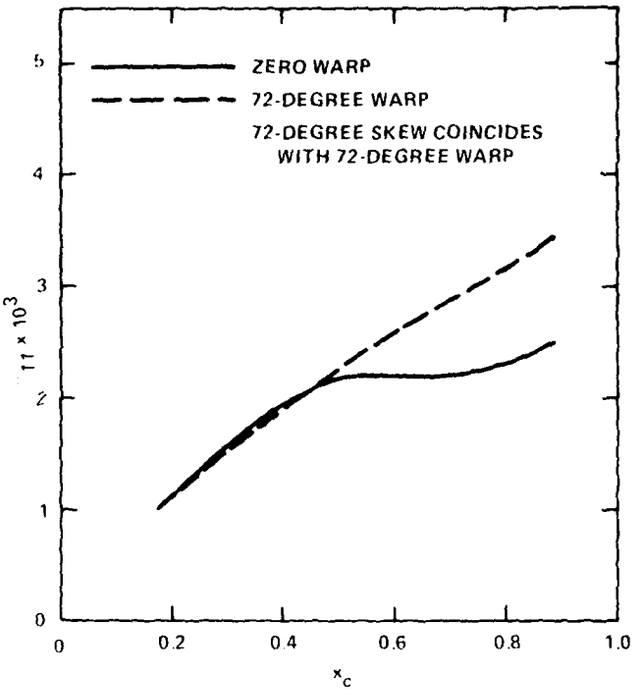

(a) SUCTION SURFACE

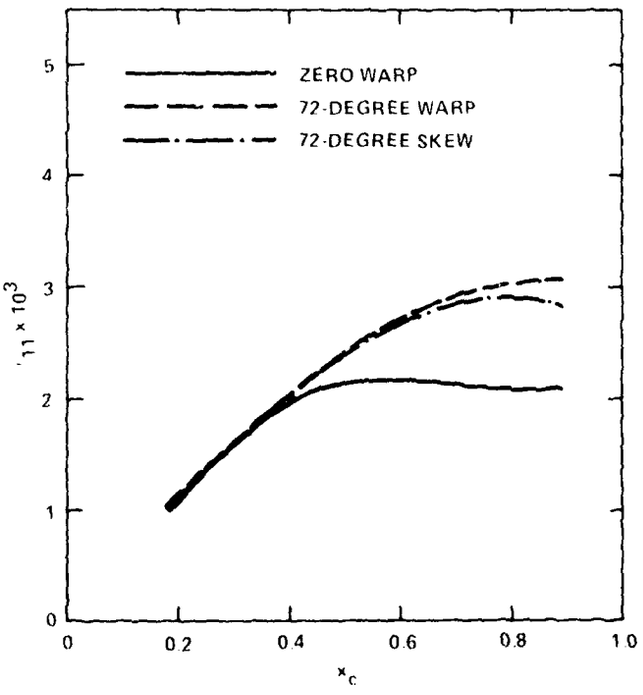

(b) PRESSURE SURFACE

Figure 9. Computed Distribution of Momentum Thickness θ_{11} Along Streamline 14 of Warped and Unwarped Blades.

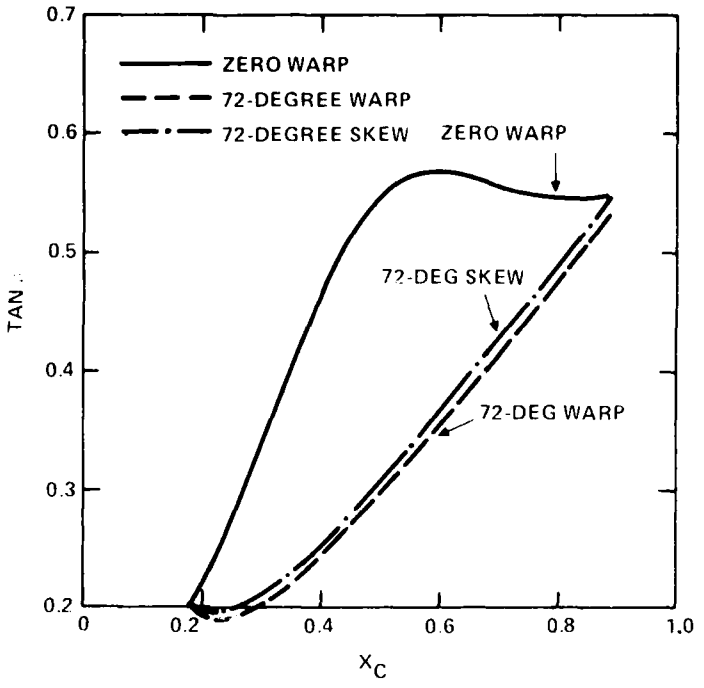

(a) SUCTION SURFACE

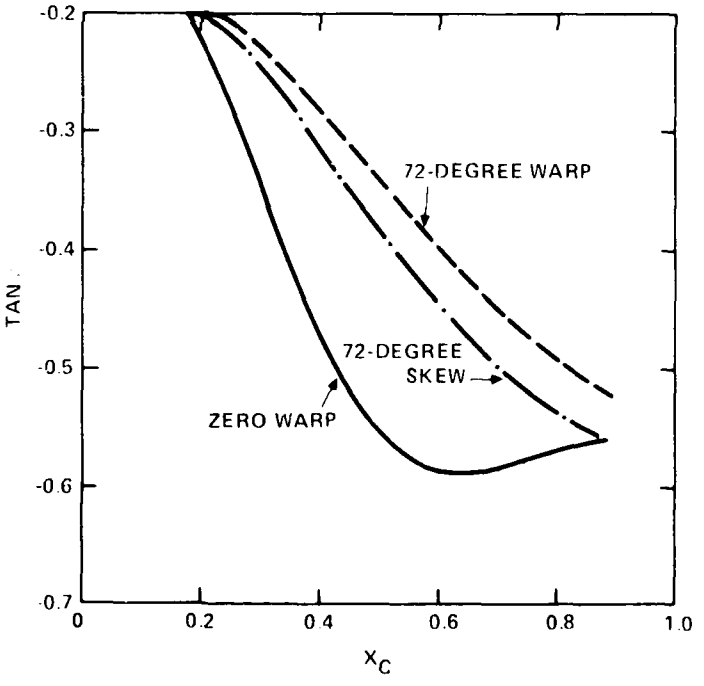

(b) PRESSURE SURFACE

Figure 10. Computed Distribution of Tangent of Limiting Streamline Angle β Along Streamline 14 of Warped and Unwarped Blades.

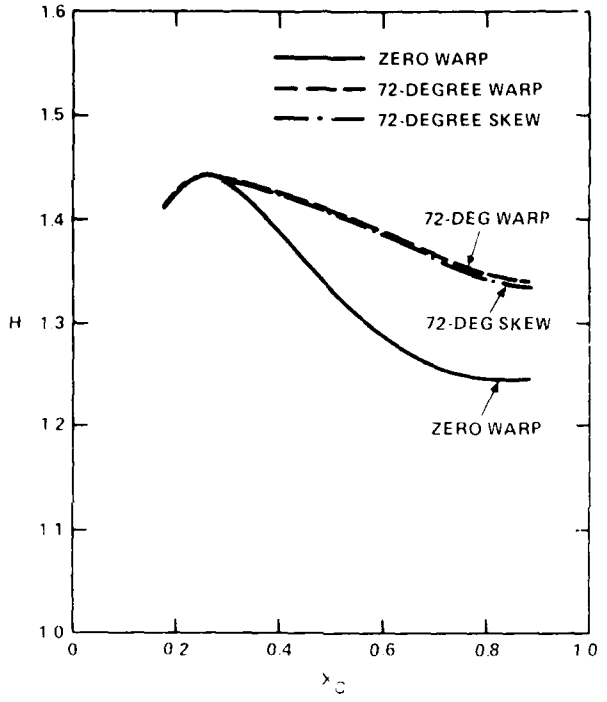

(a) SUCTION SURFACE

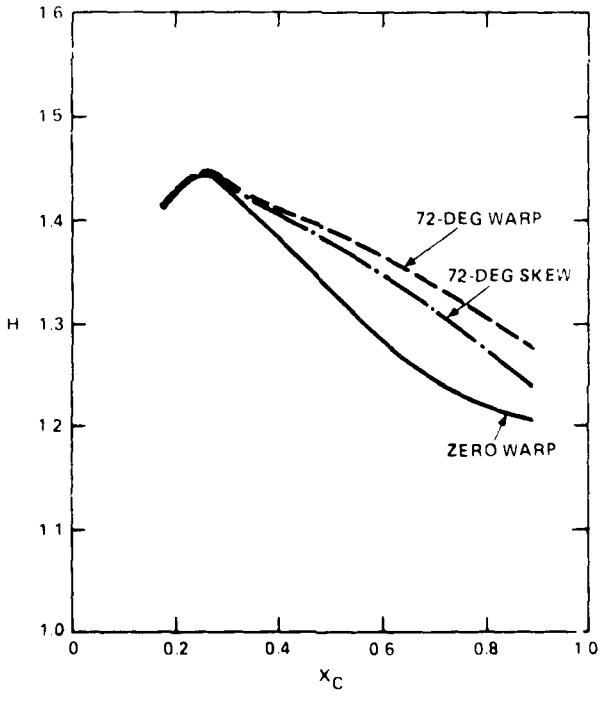

(b) PRESSURE SURFACE

Figure 11. Computed Distribution of Shape Parameter H Along Streamline 14 of Warped and Unwarped Blades.

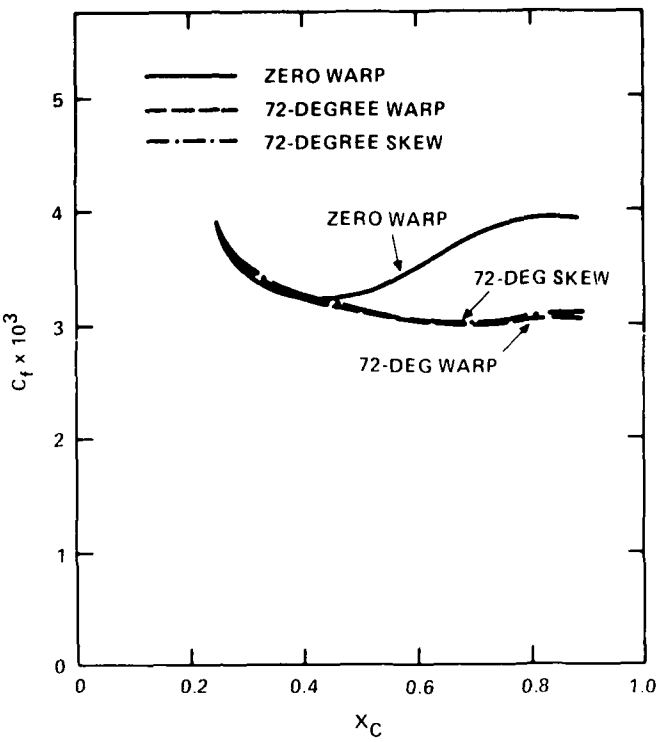

(a) SUCTION SURFACE

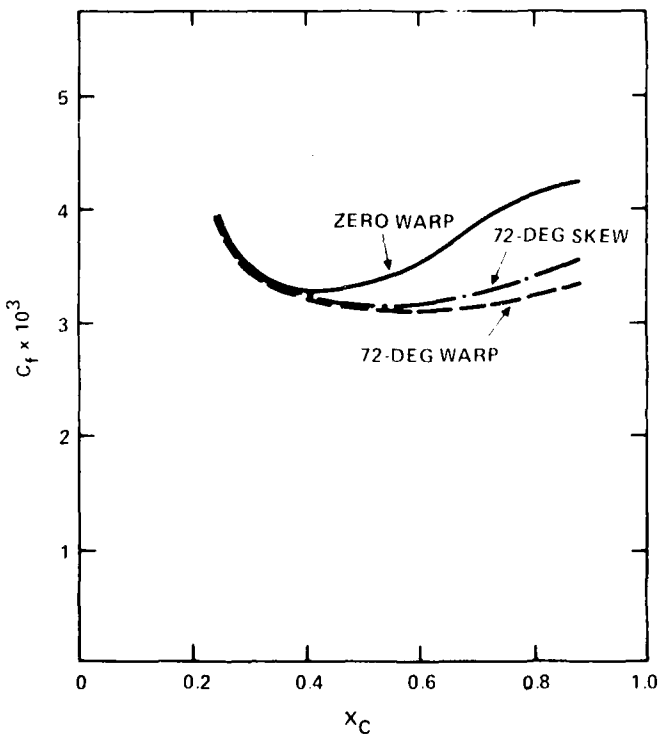

(b) PRESSURE SURFACE

Figure 12. Computed Distribution of Local Skin Friction Coefficient C_f Along Streamline 14 Warped and Unwarped Blades.

tions of up to 30-percent are predicted near the trailing edge. Similar reductions are predicted for each streamline. Small variations in the predicted values of the potential flow velocity for the various blade designs do not significantly effect these results. Since insufficient data are computed to permit a calculation of total blade drag, an average reduction of 15-percent was employed for the average chordwise blade-section drag relative to a constant drag coefficient of 0.0085. Thrust loading coefficient and power coefficient increased by one-half-percent and reduced by one-percent, respectively, hence an increase of efficiency of about two-percent for a warped or skewed blade. The actual change in efficiency was 1 percentage point.

Several calculations were made to identify the factors contributing to the predicted reduction in skin friction with increased blade warp or skew. Calculations to date seem to indicate that these differences arise from geometrical effects. Relative to the unskewed blade, the potential flow velocity decreases by less than 2 percent and the metric coefficient h_1 decreases by 10 to 20 percent for both the highly-warped and the highly-skewed blades. The metric coefficient h_2 increases by 10 to 15 percent for the warped blade and by 2 to 3 percent for the skewed blade. A reduction is predicted in the angular velocity component of 9 to 14 percent for the warped blade and of only 1 to 3 percent for the skewed blade. Thus, it does not appear as though any single factor is responsible for the predicted skin friction reduction with increased blade warp or skew. Instead, the interaction of various geometrical factors seems to contribute to this reduction.

CONCLUDING REMARKS

This paper presents analysis and results for computing three-dimensional turbulent boundary layers on the surface of a rotating blade using a momentum-integral method. The analytical and numerical procedures for solving the momentum-integral boundary-layer equations have been presented and implemented in an efficient computer code. Typical boundary-layer computations require less than 10 seconds CPU on the high-speed Burroughs 7700 computer at a cost less than one dollar. The predicted boundary-layer parameters are shown to give reasonable agreement with experimental data for a simple body. Assuming initial boundary-layer characteristics determined by flat-plate values for turbulent flow, increasing blade warp is

predicted to decrease the local skin friction coefficient. The reduction in skin friction increases the thrust coefficient and reduces the torque coefficient yielding an increased efficiency of about two percent (one percentage point). However, the accuracy of the initial values and the effect of their variation on the predicted results is not known.

Future work in this area should include an improved crossflow velocity profile, better estimation of the initial conditions for the turbulent boundary-layer calculation, and the calculation of thrust and torque to predict drag. Experimental boundary-layer data are needed to fully assess and improve the present analytical work. Future work should also include the prediction of laminar-flow characteristics at the leading edge, laminar-to-turbulence transistion predictions, and eventually the prediction of separation phenomena both on the blade surface and at the tip where a tip-vortex forms. Pioneering work on the tip region has been published by Shamroth, et al.[31]

ACKNOWLEDGMENTS

This work was funded under the DTNSRDC work unit 1500-104, Task Area SF43421001, Program Element 62543N.

The author would like to thank Dr. Christian von Kerczek, Dr. Terry Brockett, and Dr. Thomas T. Huang for their continuous support and technical guidance.

REFERENCES

1. T. von Kármán, "On Laminar and Turbulent Friction," N.A.C.A. Tech. Mem. 1092, 1946.
2. W.H. Banks and G.E. Gadd, "A Preliminary Report on Boundary Layers on Screw Propellers and Simpler Rotating Bodies," Nat. Physics Lab. Report SHR27, 1962.
3. K. Meyne, "Investigation of Propeller Boundary-Layer Flow and Friction Effect on Propeller Characteristics," Jahrbuch der Schiffbautechnischen Gesellschaft, Band 66, 1972.
4. T-S. Cham and M.R. Head, "The Turbulent Boundary-Layer Flow on a Rotating Disk," J. Fluid Mech., Vol. 37, Part 1, pp. 129-147, 1969.
5. T-S. Cham and M.R. Head, "The Turbulent Boundary Layer on a Rotating Cylinder in an Axial Stream," J. Fluid Mech., Vol. 42, Part 1, pp. 1-5, 1970.
6. T-S. Cham and M.R. Head, "The Turbulent Boundary Layer on a Rotating Nose-Body," The Aeronautical Quarterly, 1971.
7. W.C. Reynolds and T. Cebici, "Calculation of Turbulent Flow," in Topics in Applied Physics, Vol. 12, P. Bradshaw, editor, Springer-Verlag, 1976.
8. D.F. Myring, "An Integral Prediction Method for Three-Dimensional Turbulent Boundary Layers in Incompressible Flow," Royal Aircraft Establishment, Technical Report 70147, 1970.
9. B. Lakshminarayana, et al., "Turbulent Boundary Layer on a Rotating Helical Blade," J. Fluid Mech., Vol. 51, Part 3, pp. 545-569, 1972.

10. P.D. Smith, "Calculation Methods for Three-Dimensional Turbulent Boundary Layers," A.R.C. Reports and Memoranda No. 3523, 1966.

11. N.A. Cumpsty and M.R. Head, "The Calculation of Three-Dimensional Turbulent Boundary Layers, Part 1: Flow Over the Rear of an Infinite Swept Wing," The Aeronautical Quarterly, Vol. 18, pp. 55-84, 1965.

12. P.S. Granville, "Integral Methods for Turbulent Boundary Layers in Pressure Gradients," Journal of Ship Research, 1972.

13. T. Brockett, "Lifting-Surface Hydrodynamics for Design of Rotating Blades," Paper presented at "Propellers '81 Symposium," SNAME, May 1981.

14. R.W. Hamming, Introduction to Applied Numerical Analysis, McGraw-Hill Book Company, New York, 1971.

15. D.G. Schweikert, "An Interpolation Curve Using a Spline in Tension," J. Math. Physics. 45, pp. 312-317, 1966.

16. A.R. Mitchell, Computational Methods in Partial Differential Equations, John Wiley and Sons, New York, 1969.

17. F.K. Moore, Theory of Laminar Flows, Princeton University Press, New Jersey, 1964.

18. C. von Kerczek and T.J. Langan, "An Integral Prediction Method for Three-Dimensional Turbulent Boundary Layers on Ships," DTNSRDC Report 79/006, 1979.

19. M.R. Head, "Entrainment in the Turbulent Boundary Layer," A.R.C. Reports and Memoranda 3152, 1958.

20. B.G.J. Thompson, "A New Two-Parameter Family of Mean Velocity Profiles for Incompressible Boundary Layers on Smooth Walls," A.R.C. Reports and Memoranda 3463, 1965.

21. M.R. Head and V.C. Patel, "Improved Entrainment Method for Calculating Turbulent Boundary Layer Development," A.R.C. Reports and Memoranda 3643, 1968.

22. M.A. Cooke, "A Calculation Method for Three-Dimensional Turbulent Boundary Layers," A.R.C. Reports and Memoranda 3199, 1961.

23. V.C. Patel, "A Simple Integral Method for the Calculation of Thick Axisymmetric Turbulent Boundary Layers," The Aeronautical Quarterly, Vol. 25, 1974.

24. R.E. Wallace, "The Experimental Investigation of a Swept-Wing Research Model Boundary Layer," Aerodynamic Report of the Municipal University of Wichita, 1953.

25. A. Mager, "Generalization of Boundary-Layer Momentum-Integral Equations to Three-Dimensional Flows, Including Those of Rotating Systems," National Advisory Committee for Aeronautics Report 1067, 1952.

26. J.E. Green, et al., "Prediction of Turbulent Boundary-Layers and Wakes in Compressible Flow by a Lag-Entrainment Method," A.R.C. Reports and Memoranda 3791, 1977.

27. L. Prandtl, Ergeb. AVA Goett., Ser. III, pp. 1-5, 1927.

28. K.E. Schoenherr, "Resistance of Flat Surfaces Moving Through a Fluid," Trans. SNAME 40, p. 279, 1932.

29. F.M. White, Viscous Fluid Flow, McGraw-Hill, Inc., New York, 1974.

30. T. Cebeci and A.M.O. Smith, Analysis of Turbulent Boundary Layers, Academic Press, New York, 1974.

31. S.J. Shamroth, "A Viscous Flow Analysis for the Tip Vortex Generation Process," NASA CR3184, 1979.

APPENDIX

COMPUTATIONAL RESULTS FOR BLADES 2 AT A FULI-SCALE REYNOLDS NUMBER

The turbulent boundary layer results for Blades 2 (unskewed Blade 2A, 72 degree warped Blade 2B, and 72 degree skewed Blade 2C) presented in the main text are computed for a model-scale 0.7 radius Reynolds number of 4×10^6. In this appendix, similar results are presented for these blades for a full-scale 0.7 radius Reynolds number of 6×10^7. The assumed flow conditions are $\nu = 1.191 \times 10^{-6}$ m^2/s (1.282×10^{-5} ft^2/sec), V = 16.9 m/s (55.3 ft/sec), and ω = 26.1 rad/sec. The propeller diameter is 4.572 m (15 ft).

A finer computation grid was selected for the full-scale computations. More grid nodes were added in the radial direction in order to compute the boundary layer characteristics closer to the hub at the trailing edge of the blade. The boundary layer results on the model-scale blades were also recomputed using the finer grid. Both full-scale and model-scale results are given in this appendix.

Again, initial conditions for the streamwise momentum thickness θ_{11} and the shape factor H are assumed to be determined by flat-plate values for turbulent flow[28,29,30] as described in the main text. The value of the limiting streamline angle β is also given by the rotating disk value of β = +11 degrees on the blade suction surface and β = -11 degrees on the blade pressure surface. Since no previous analytical or experimental data exist for these blades and the starting conditions are at best a guess, the computed results can be considered only qualitatively valid.

Since the local skin friction coefficient C_f contributes to the overall drag, it is, perhaps, the boundary layer result of most interest. Therefore, the only comparison presented is that of the skin friction coefficient at the 0.73-radius for the three blades at both model-scale and full-scale. Figure 13 shows the computed percentage change in C_f for Blades 2B and 2C from the unskewed Blade 2A. The open symbols represent the full-scale results and the solid symbols represent the model-scale results. As shown in Figure 13a, a decrease in the skin friction coefficient is predicted on the suction surface at both scales for the warped and skewed blades. The decrease in C_f continues to the trailing edge of the blades. There is also little variation in the results for warp and skew at each scale. Slightly larger changes in C_f are predicted for the model-scale blades than for the full-scale blades. Figure 13b shows the changes in the local skin friction coefficient on the pressure surface of the blades. Again, a decrease in C_f is predicted at both full-scale and model-scale for blade warp and blade skew. However, at the trailing edge of the

blade, C_f varies little from the value predicted for the unskewed Blade 2A. Blade skew is shown in Figure 13b to have a smaller effect on C_f than blade warp. Overall, Figure 13 shows that blade warp and blade skew are predicted to decrease the local skin friction coefficient C_f.

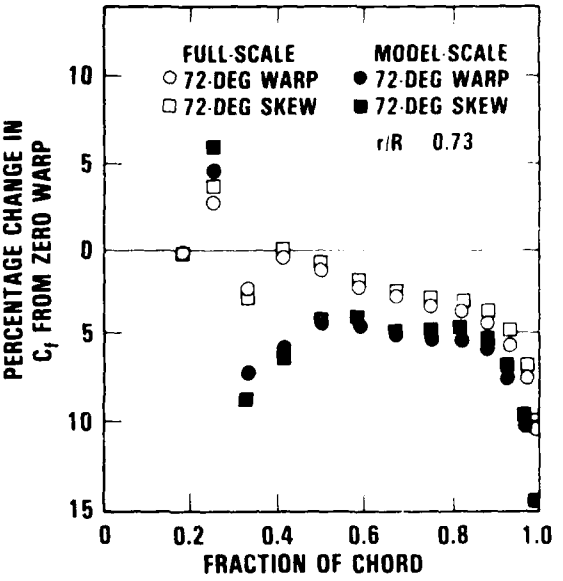

(a) SUCTION SURFACE

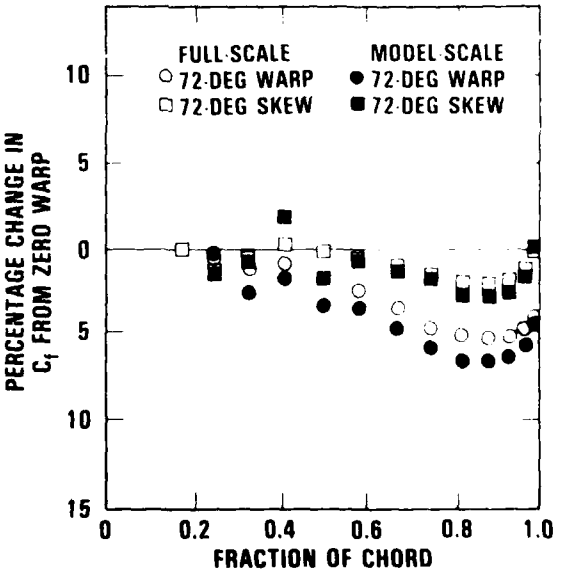

(b) PRESSURE SURFACE

Figure 13. Effect of Warp and Skew on Predicted Values of Local Skin Friction Coefficient C_f

INITIAL DISTRIBUTION

Copies	
6	ONR
	1 438
	1 492
	1 Power Branch
	1 (Branch Office, Pasadena, CA) (R.J. Marcus)
	1 (Branch Office, Chicago, IL)
	1 (Branch Office, Boston, MA)
1	USNA ANNA
1	NAVPGSCOL (A.E. Fuhs)
3	NOSC
	1 6342
	1 2542
	1 Lib
1	NSWC/Lib
12	NAVSEA
	1 03D
	1 05H
	1 09G32 (Lib)
	1 31R
	1 3121
	1 32
	1 3213
	1 52B
	1 52P
	1 521
	1 524
	1 63R31
12	DTIC
2	MIT
	1 J. Kerwin
	1 P. Leehey
2	PSU/ARL
	1 R. Henderson
	1 W. Gearhart
2	SIT
	1 J. Breslin
	1 Lib

Copies	
1	UNIV OF CA
1	UNIV OF MI (T.J. Ogilvie)
1	UNIV OF IO (L. Landweber)
1	UNIV OF MS (J.A. Fox)
2	Webb Inst
	1 L.W. Ward
	1 Lib
1	Hydrodynamics Research Asso
1	Hydronautics, Inc.

CENTER DISTRIBUTION

Copies	Code	Name
1	1500	W.E. Morgan
1	1504	V.J. Monacella
1	1507	D.S. Cieslowski
1	152	W.C. Lin
1	1524	W.G. Day
1	1528	M. Wilson
1	154	J.H. McCarthy
1	1543	R. Cumming
1	1544	T. Brockett
1	1544	R. Boswell
1	1544	G.F. Lin
1	1544	D. Nigro
1	1544	G. Platzer
1	1544	S. Jessup
1	1552	T.T. Huang
10	1552	N. Groves
1	1552	J. Libby
1	1552	Y. Shen
1	1556	G. Santore
1	1556	D. Coder
1	1556	E. Rood

PRECEDING PAGE BLANK-NOT FIL

CENTER DISTRIBUTION (Continued)

Copies	Code	Name
1	1606	T.C. Tai
1	184	J. Schot
1	1843	H. Haussling
1	19	M. Sevik
1	1905.1	W.K. Blake
1	194	J. Shen
1	196	D. Feit
1	2721	J.G. Stricker
10	5211.1	Reports Distribution
1	522.1	Unclass Lib (C)
1	522.2	Unclass Lib (A)

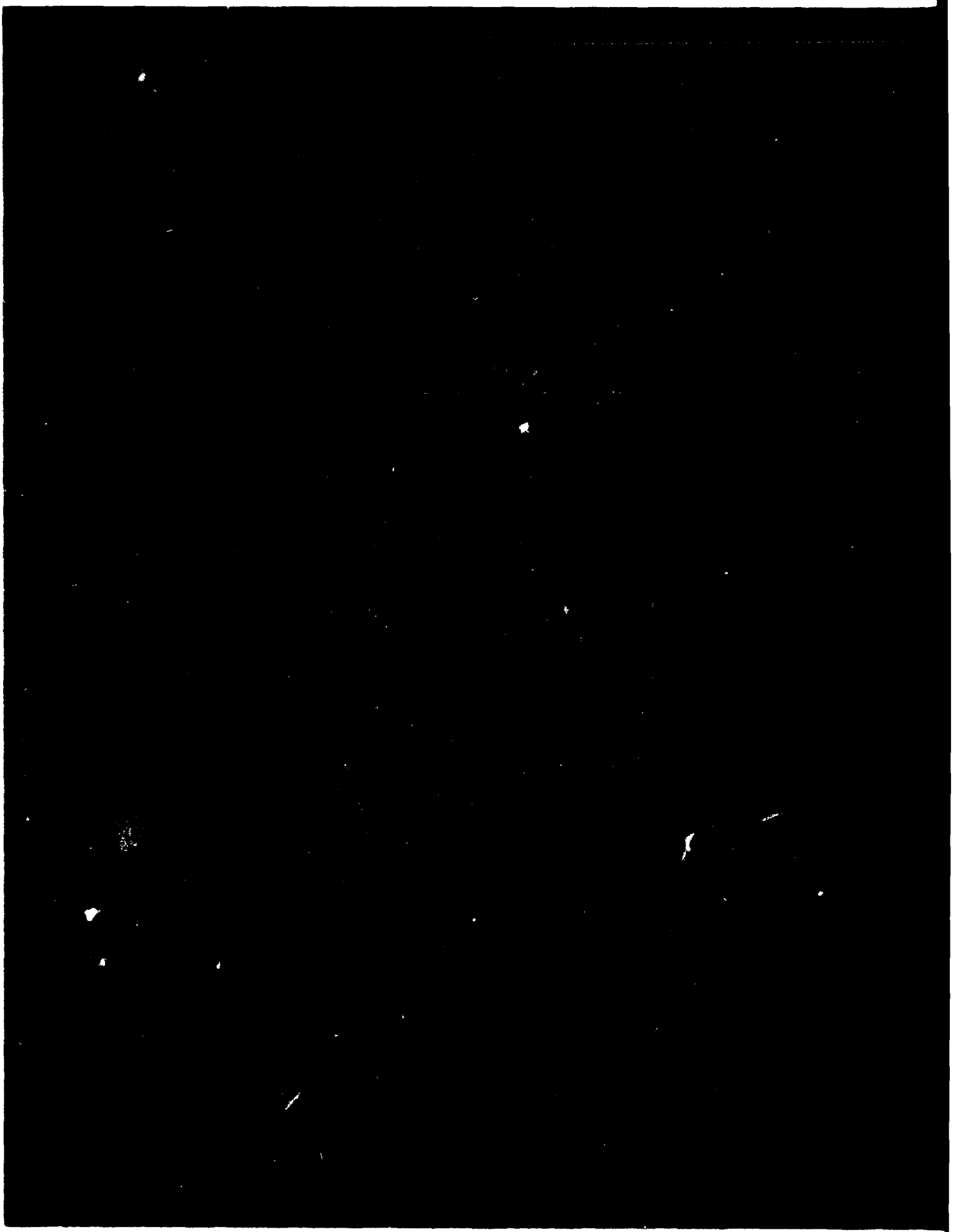

DATE
FILMED
8